Preprints.org

Article

Not peer-reviewed version

Deciphering the Regulatory Role of Terrain Conditions in the Vegetation-Climate Interactions Across China

Minqian He and Hailong Wang *

Posted Date: 12 February 2026

doi: 10.20944/preprints202602.1018.v1

Keywords: Gross Primary Productivity (GPP); climate change; topographic regulation; non-linear thresholds; Structural Equation Modeling (SEM)

Preprints.org is a free multidisciplinary platform providing preprint service that is dedicated to making early versions of research outputs permanently available and citable. Preprints posted at Preprints.org appear in Web of Science, Crossref, Google Scholar, Scilit, Europe PMC.

Copyright: This open access article is published under a Creative Commons CC BY 4.0 license, which permit the free download, distribution, and reuse, provided that the author and preprint are cited in any reuse.

Preprints.org (www.preprints.org) | NOT PEER-REVIEWED | Posted: 12 February 2026 doi:10.20944/preprints202602.1018.v1

Disclaimer/Publisher's Note: The statements, opinions, and data contained in all publications are solely those of the individual author(s) and contributor(s) and not of MDPI and/or the editor(s). MDPI and/or the editor(s) disclaim responsibility for any injury to people or property resulting from any ideas, methods, instructions, or products referred to in the content.

Article

Deciphering the Regulatory Role of Terrain Conditions in the Vegetation-Climate Interactions Across China

Minqian He [1,2] and Hailong Wang [1,2,*]

[1] School of Civil Engineering, Sun Yat-sen University, Guangzhou, China, 510275

[2] Center for Water Resources and Environment Research, Sun Yat-sen University, Guangzhou, China, 510275

* Correspondence: wanghlong3@mail.sysu.edu.cn

Highlights

What are the main findings?

Precipitation explains 72.5% of GPP spatial heterogeneity across China, and its influence is strongly amplified by terrain conditions which is often overlooked.

Critical thresholds for terrain and climate interactions are identified, providing quantifiable benchmarks for predicting ecosystem shifts under environmental change.

What are the implications of the main findings?

Terrain modulates the impacts of key climate factors on GPP through complex hydrothermal redistribution processes, and an altitudinal transition from water to temperature controlling mechanism is revealed for the benefit of ecosystem management.

The findings underscore the necessity of incorporating terrain-mediated, non-linear climate effects into regional ecological models to improve accuracy.

Abstract

Terrestrial Gross Primary Productivity (GPP) is pivotal to the global carbon cycle, and its response to climate change is strongly regulated by topographic conditions through complex, non-linear mechanisms that remain poorly quantified at macro scales. Integrating multi-source remote sensing data with structural equation modeling (SEM), geographical detectors, and generalized additive models (GAM), this study investigated the spatiotemporal dynamics of GPP and its non-linear responses to coupled climate-topography gradients across China from 2001 to 2020. Results revealed a significant increasing trend in GPP across nearly 80% of China, with precipitation identified as the dominant driver, surpassing temperature and radiation. Topography significantly modulated climate sensitivity by redistributing hydrothermal resources. A distinct transition in dominant limiting factors was observed along the altitudinal gradient, shifting from water-limited (<2000 m) to energy-limited (>3000 m) regimes. Notably, mid-altitude regions (1000–2000 m) exhibited the highest sensitivity to precipitation, representing an ecological "sweet spot". Furthermore, we quantified critical ecological thresholds for climatic drivers, identified saturation points for temperature (~17.4°C) and precipitation (~1974 mm), and an inhibition threshold for solar radiation (>101 W/m²). These findings elucidate the transition mechanisms of climatic constraints and non-linear thresholds in complex terrain, providing robust scientific evidence for region-specific ecosystem and carbon management.

Keywords: Gross Primary Productivity (GPP); climate change; topographic regulation; non-linear thresholds; Structural Equation Modeling (SEM)

© 2025 by the author(s). Distributed under a Creative Commons CC BY license.

Preprints.org (www.preprints.org) | NOT PEER-REVIEWED | Posted: 12 February 2026 doi:10.20944/preprints202602.1018.v1

1. Introduction

Terrestrial vegetation plays a pivotal role in climate mediation and ecological balance [1,2]. This vital function as a persistent global carbon sink can be fundamentally quantified by Gross Primary Productivity (GPP), the core metric of the terrestrial ecosystem's CO2 absorption capacity [3,4]. However, GPP dynamics are not isolated but tightly coupled to a complex system involving plant physiology, climatic and topographic factors [5], resulting in responses characterized by high complexity, non-linearity, and significant spatiotemporal heterogeneity [6]. Given China's vast territory, complex terrain, and highly diverse climate [7], its vegetation dynamics exhibited pronounced regional differentiation and diverse response mechanisms [8,9]. Therefore, a systematic investigation into the complex drivers and underlying mechanisms of GPP dynamics is essential for scientifically managing cross-climatic zone ecosystems and refining global carbon budget estimations.

Climate change poses a major threat to all Earth systems, with a continuous increase in mean surface temperature [10]. Investigating the vegetation-climate relationship is therefore a critical foundation for China's long-term environmental sustainability and the success of its ecological restoration efforts [11]. Extensive research across China has confirmed a widespread increasing trend in vegetation productivity [12,13], where precipitation and temperature are widely regarded as the most crucial climatic factors controlling vegetation growth [14]. With the vegetation change closely associated with improved hydrothermal conditions [15,16], research argues that the influence of solar radiation cannot be overlooked [17]. This has led to extensive discussion regarding the combined effects of these drivers. For instance, some studies revealed complex regional characteristics, such as precipitation enhancing desert vegetation while temperature showing positive correlations in other areas [11]; others indicated that radiation and precipitation dominated regional vegetation growth [18], or that their combined effects drove significant vegetation growth rate [19]. This extensive pool of research, however, has produced a fragmented and sometimes contradictory understanding of dominant driver attribution. For example, some large-scale studies [20] found that rainfall had a greater overall control over vegetation dynamics than radiation and temperature. Conversely, regional-scale analyses [21] concluded that temperature was the primary climatic factor. Such inconsistency is not merely a reflection of regional differentiation, it might expose a systemic methodological limitation. A core challenge is that the climatic drivers of precipitation, temperature, and radiation are non-independent and subject to collinearity [22]. Consequently, many traditional statistical methods that rely on linear assumptions often struggle to rigorously isolate their individual effects [23,24], leading to this fragmented and conflicting understanding of attribution.

Although climatic factors are widely regarded as the dominant drivers of vegetation change, this perspective often neglects the critical modulatory effect of topographic characteristics. Topography (such as altitude, slope, and aspect) fundamentally governs regional microclimate, soil hydrothermal redistribution, and material transport, thereby altering the GPP-climate interactions [25–27]. China's vast territory and complex terrain result in significant vertical gradients, leading to pronounced differences in water and heat conditions across various land surfaces. A number of regional studies have begun to explore this complexity, e.g., Zhang et al. [28] investigated the multidimensional variation of vegetation NDVI (Normalized Difference Vegetation Index) along topographic gradients, and noted that high-altitude areas were mainly controlled by precipitation; Wang et al. [29] constructed a Topographic Comprehensive Index (TCI) and found that at small scales altitude controls the horizontal distribution of vegetation, while slope and aspect co-regulate the distribution pattern by influencing factors such as radiation; Zou et al. [30] established a terrain model and found that mountain height, aspect, and climate jointly modulated the upper limit of vegetation growth in alpine ecosystems. While these valuable regional studies confirm the existence of topographic modulation, they also reveal that current knowledge remains fragmented and a consistent large-scale quantification is still lacking [31]. This gap is particularly evident in, but not limited to, China's complex mountain systems, where the synergistic controls of elevation and climate remain insufficiently quantified and specific local characteristics have not been well investigated [32,33].

© 2025 by the author(s). Distributed under a Creative Commons CC BY license.

Preprints.org (www.preprints.org) | NOT PEER-REVIEWED | Posted: 12 February 2026 doi:10.20944/preprints202602.1018.v1

More broadly, many large-scale studies ignore these topographic effects entirely, while research that does consider topography often simplifies it to just elevation, leaving the complex interactions between slope, aspect, and elevation significantly understudied [34]. Therefore, current research lacks quantified evidence to determine the explicit transition mechanism of dominant limiting factors along these major topographic gradients at a systematic, national scale, addressing a key mechanistic and quantitative gap.

In complex ecosystem analyses, quantifying the influence of long-term climatic and topographic effects on vegetation indices is critical in determining the optimal characteristics of key natural drivers of vegetation growth [35]. However, most previous studies remained at the level of correlational analysis, failing to fully reveal the intricate causal structure between climate, topography, and vegetation [36]. Traditional statistical methods often struggled to effectively distinguish between the direct effects of climatic drivers and the indirect cascading effects induced by topographic modulation. However, there are advanced methods that can be employed to address these issues. For instance, models like Geodetector [37,38] and Partial Least Squares Structural Equation Modeling (PLS-SEM) [39,40]have successfully moved beyond simple correlation to reveal complex interactions and distinguish between the direct effects of climatic drivers and the indirect effects induced by topographic modulation. Guo et al. [41] demonstrated that the interaction of any two factors drove NDVI changes more strongly than their individual effects alone. Kang et al. [42] applied the Principal Component Analysis (PCA) and PLS-SEM and found that temperature and precipitation were the primary drivers of vegetation growth, while altitude indirectly inhibited growth by regulating temperature and precipitation. However, a more fundamental limitation persists, i.e., even these advanced causal analyses often do not account for the inherently non-linear and non-monotonic nature of ecological responses. This is a critical omission, as increasingly frequent and intense climate extreme events [10] mean that the influence of climatic factors is not monotonic, but varies within a potential range or threshold [43]. As Piao et al. [44] and Beigaitė et al. [45] demonstrated, crossing these thresholds can lead to abrupt changes in ecosystem response, such as saturation or inhibition. Consequently, the precise quantification of these non-linear saturation or inhibition thresholds is urgently required [46]. Despite this urgency, our understanding of the occurrence and consequences of such thresholds remains limited, and quantifying them can be challenging [47], representing a critical, unresolved frontier in ecosystem science.

This study combines remote sensing data with meteorological and topographic information to comprehensively explore the complex, non-linear, and topographically modulated influence of climate and terrain conditions on China's terrestrial ecosystem between 2001 and 2020. To address the comprehensive research gaps identified above, the specific objectives were (1) to quantify the spatial-temporal dynamics of GPP and key climatic factors, resolving the contradictory attributions by identifying the dominant climate factors boosting or inhibiting vegetation productivity across China's diverse ecoregions; (2) to evaluate the divergent regulatory effects of topographic factors on the GPP-climate relationship and quantify the transition mechanism of dominant limiting factors along major topographic gradients; and (3) to determine the ecological saturation and inhibition thresholds of GPP to key climatic drivers, thereby enhancing our understanding of the non-linear response characteristics of GPP in the context of climate change. The findings of this study will provide a mechanistic, parameterizable understanding of ecosystem response, offering robust scientific evidence for formulating effective region-specific carbon sequestration and ecological protection policies.

2. Materials and Methods

2.1. Data Sources and Preprocessing

This study applied four categories of data, i.e., GPP, meteorological data, land cover data, and topographic data. All datasets were processed for the period 2001-2020 due to their common availability. To ensure spatial consistency for analysis, all datasets were resampled to a uniform

© 2025 by the author(s). Distributed under a Creative Commons CC BY license.

Preprints.org (www.preprints.org) | NOT PEER-REVIEWED | Posted: 12 February 2026 doi:10.20944/preprints202602.1018.v1

spatial resolution of 0.1°×0.1° to match the meteorological data. The GPP data [48] were sourced from the Global 8-day 0.05-degree GOSIF GPP product. This dataset is derived from OCO-2 SIF data and other satellite products, offering high accuracy in capturing vegetation productivity [49,50]. The original 0.05° data were resampled to 0.1° using bilinear interpolation method to preserve spatial gradients. The monthly climate data including precipitation, temperature, and solar radiation were obtained from the China Meteorological Forcing Data (CMFD) dataset provided by the National Tibetan Plateau Data Center (https://www.tpdc.ac.cn). This dataset has a native spatial resolution of 0.1°. We directly utilized the annual total precipitation (derived from monthly sums) and annual mean temperature and radiation (derived from monthly averages) for our analysis. Land cover classification was based on the 30-meter annual China Land Cover Dataset (CLCD, https://zenodo.org/records/8176941). We used the 2010 CLCD product as a representative baseline for the study period. The land cover data were resampled to 0.1° grids using the nearest neighbor resampling method. This study focused on the four dominant vegetated types only, i.e., cropland, forest, shrubland, and grassland. Digital Elevation Model (DEM) data were derived from the SRTM (Shuttle Radar Topography Mission) Version 4 (https://srtm.csi.cgiar.org) with a 90-meter resolution. To correctly derive terrain metrics, slope and aspect were first calculated from the 90-meter native-resolution DEM, and then they were all resampled to 0.1° using bilinear interpolation for further analysis.

2.2. Data Analysis Methods

To systematically quantify the spatiotemporal dynamics of GPP and unravel its complex drivers, this study employed a multi-stage analytical framework (Figure 1). Each method is detailed below.

Figure 1. Schematic multi-stage analytical framework adopted in this study.

2.2.1. Trend Analysis

To investigate the spatiotemporal trends of GPP and key climatic factors across China, this study employed the non-parametric Mann-Kendall trend test combined with Sen's slope estimator.

(1) Mann-Kendall trend test

The Mann-Kendall test is a non-parametric statistical method that does not require data to follow specific distributions and is insensitive to outliers, making it suitable for analyzing long-term time series trends. The test statistic S is calculated as follows:

© 2025 by the author(s). Distributed under a Creative Commons CC BY license.

Preprints.org (www.preprints.org) | NOT PEER-REVIEWED | Posted: 12 February 2026 doi:10.20944/preprints202602.1018.v1

$$S = \sum_{i=1}^{n-1} \sum_{j=i+1}^{n} sgn(x_j - x_i) \quad (1)$$

where x_j and x_i represent observations from years *j* and *i* respectively, n denotes the time series length (n=20 in this study), and *sgn* is the sign function:

$$sgn(x) = \begin{cases} 1 & x > 0 \\ 0 & x = 0 \\ -1 & x < 0 \end{cases} \quad (2)$$

When n≥8, the statistic *S* approximately follows a normal distribution, with its variance calculated as:

$$Var(S) = \frac{n(n-1)(2n+5)}{18} \quad (3)$$

The standardized test statistic *Z* is computed as:

$$Z = \begin{cases} \frac{S-1}{\sqrt{Var(S)}} & S > 0 \\ 0 & S = 0 \\ \frac{S+1}{\sqrt{Var(S)}} & S < 0 \end{cases} \quad (4)$$

(2) Sen's slope estimator

Sen's slope estimator quantifies the magnitude of trends by calculating the median of all pairwise slopes:

$$\beta = \text{median}\left(\frac{x_j - x_i}{j - i}\right) \quad \forall i < j \quad (5)$$

where β represents Sen's slope, indicating the annual change rate of the time series.

(3) Trend classification criteria

Based on the significance of Mann-Kendall test (α=0.05) and the magnitude of Sen's slope, pixel-level trends were categorized into five classes (Table 1).

Table 1. Trend classification based on Mann-Kendall test and Sen's slope estimator.

Change Type	Sen's slope	|Zs|
Significant Improvement	β ≥ 0.0005	> 1.96
Significant Degradation	β≤ -0.0005	> 1.96
Slight Improvement	β≥ 0.0005	≤ 1.96
Slight Degradation	β≤ -0.0005	≤ 1.96
Stable	-0.0005 <β< 0.0005	≤ 1.96

2.2.2. Partial Correlation Analysis

To eliminate the interference among climatic factors and reveal the independent relationships between GPP and individual climatic factors, this study employed partial correlation analysis. This method quantifies the net correlation between two variables while controlling for the linear effects of other variables. The second-order partial correlation coefficient is calculated as:

$$r_{xy \cdot z} = \frac{r_{xy} - r_{xz} r_{yz}}{\sqrt{(1 - r_{xz}^2)(1 - r_{yz}^2)}} \quad (6)$$

© 2025 by the author(s). Distributed under a Creative Commons CC BY license.

Preprints.org (www.preprints.org) | NOT PEER-REVIEWED | Posted: 12 February 2026 doi:10.20944/preprints202602.1018.v1

where $r_{xy \cdot z}$ is the first-order partial correlation. This analysis allowed for the determination of the direct influence of each climatic factor on GPP, independent of the others.

2.2.3. Sensitivity Response Index (SRI)

To quantify the sensitivity of GPP to long-term changes in each climatic driver, a trend-based sensitivity analysis was conducted. This method defines sensitivity as the ratio of the GPP trend to the corresponding climatic factor's trend.

First, the Theil-Sen slopes (β) were calculated for GPP (β_{GPP}) and each climate factor ($\beta_{Climatei}$). The sensitivity (SRI_i) was then computed for each pixel as:

$$SRI_i = \frac{\beta_{GPP}}{\beta_{Climate_i}} \tag{7}$$

where SRI_i is the sensitivity coefficient of GPP to climate factor i, β_{GPP} is the long-term trend slope of GPP, and $\beta_{Climatei}$ is the long-term trend slope of the climate factor i. The resulting SRI_i coefficient quantifies the change in GPP for each unit change in the climate driver over the study period.

2.2.4. Geodetector Analysis

To quantify the explanatory power of factors and their interactions on GPP's spatial heterogeneity, the Geographical Detector (Geodetector) model was used. The core of this model is the q-statistic, which measures spatial correspondence by comparing the sum of variance within strata to the total spatial variance:

$$q = 1 - \frac{\sum_{h=1}^{L} N_h \sigma_h^2}{N\sigma^2} = 1 - \frac{SSW}{SST} \tag{8}$$

where q is explanatory power of a factor (ranges from 0 to 1), L is the number of strata (categories) of the driving factor, N_h and N is the number of samples in stratum h and the total region, respectively, σ^2_h and σ^2 is the variance of GPP in stratum h and the total region, respectively. q=1 indicates the factor perfectly explains the spatial distribution of GPP. The Interaction Detector was also used to assess whether the combined effect of two factors (e.g.,q(Precipitation∩Altitude)) was stronger or weaker than their individual effects.

2.2.5. Structural Equation Model

Path Analysis, a specific form of Structural Equation Modeling (SEM), was employed to test the hypothesized causal architecture connecting topography, climate, and GPP. Based on ecological theory, we specified an a priori causal model where (a) topographic factors act as exogenous variables, (b) climate factors act as mediating variables which are influenced by topography, and (c) GPP acts as the final endogenous variable which is directly influenced by the climate mediators.

This model was estimated using a robust maximum likelihood estimator. The model's validity was assessed using Goodness-of-Fit indices including the Comparative Fit Index (CFI > 0.90), the Root Mean Square Error of Approximation (RMSEA < 0.08), and the Chi-square (X2) test (p> 0.05). Standardized path coefficients were then extracted to quantify the strength of each direct and indirect causal pathway.

2.2.6. Generalized Additive Model (GAM)

To explore the non-linear responses and identify critical ecological thresholds, Generalized Additive Models (GAMs) were employed. This study did not fit a single multivariate model. Instead, three separate univariate GAMs were fitted independently to isolate the distinct non-linear partial response curve for each driver:

$$g(E[GPP]) = \beta_0 + s_1(Temperature) + \epsilon \tag{9}$$

© 2025 by the author(s). Distributed under a Creative Commons CC BY license.

Preprints.org (www.preprints.org) | NOT PEER-REVIEWED | Posted: 12 February 2026 doi:10.20944/preprints202602.1018.v1

$$g(E[GPP]) = \beta_0 + s_2(Precipitation) + \epsilon \quad (10)$$

$$g(E[GPP]) = \beta_0 + s_3(Radiation) + \epsilon \quad (11)$$

where g· is a link function (an identity function for GPP). E [GPP] is the expected value of GPP, β0 is the intercept, s1· is the non-parametric smoothing function that captures the non-linear relationship for the given driver, ϵ is the error term. By fitting each model separately, the specific functional form of GPP's response to each climate variable could be extracted. The resulting partial response curves were then visually and quantitatively analyzed to identify critical point, such as saturation or inhibition.

3. Results

3.1. Spatial-Temporal Relationships Between GPP and Climate Factors

Between 2001 and 2020, China's regional GPP and key climatic factors (precipitation, temperature, and radiation) exhibited significant spatiotemporal variations (Figure 2), vegetation ecosystems demonstrated a clear trend of improvement. A substantial 79.3% of the national area showed an increase in GPP, with an average growth rate of 5.86 g C/m² per year (Figure 2a). This positive trend is closely linked to favorable changes in climatic conditions during the same period. Over 76% of the country experienced an increasing trend in precipitation (Figure 2b), while more than 80% of the area recorded rising temperatures (Figure 2c), collectively creating advantageous hydrothermal conditions for vegetation growth.

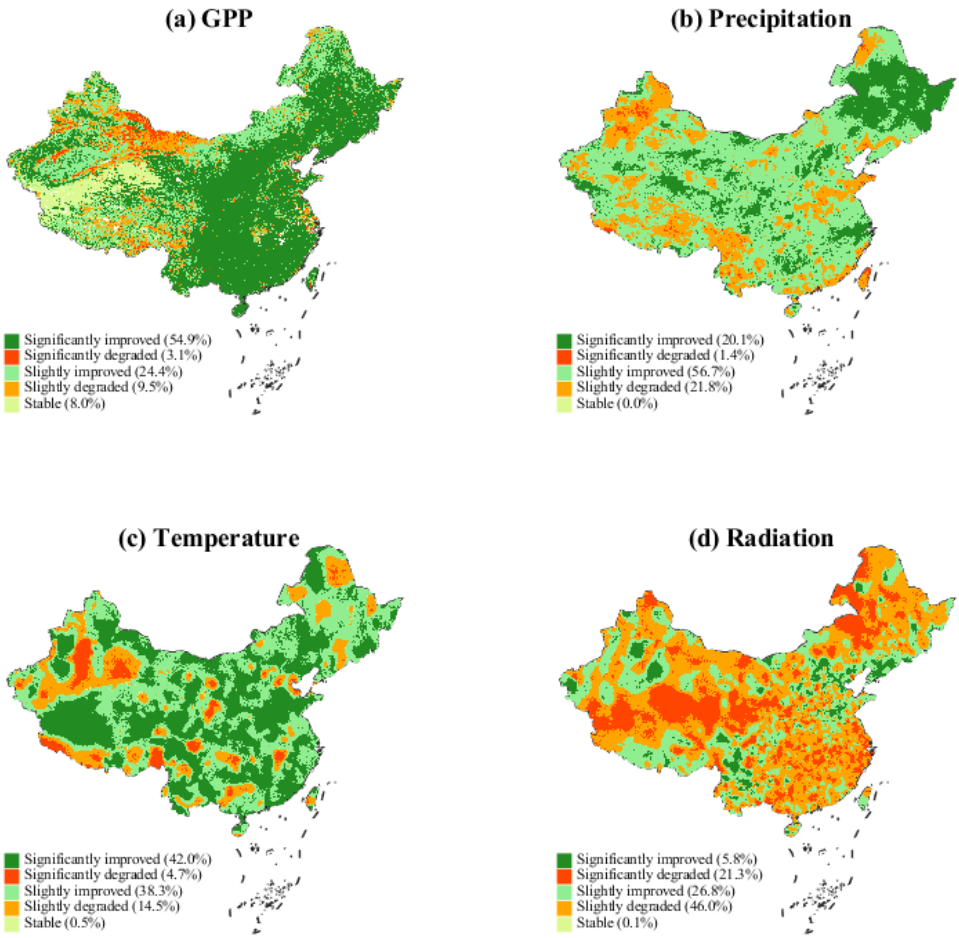

Figure 2. Spatial trends in GPP, precipitation, temperature, and solar radiation across China from 2001 to 2020. In parentheses is the areal proportion of each statistical category.

© 2025 by the author(s). Distributed under a Creative Commons CC BY license.

Preprints.org (www.preprints.org) | NOT PEER-REVIEWED | Posted: 12 February 2026 doi:10.20944/preprints202602.1018.v1

Spatially, the most significant GPP growth was concentrated in the forest and cropland areas of southeastern, northeastern, and southwestern China, where enhanced GPP was primarily driven by superior hydrothermal conditions. Conversely, broad regions across northern and northwestern China showed a degradation trend in GPP. This decline is strongly associated with potential drought stress resulting from reduced local precipitation and rapid temperature increases. Notably, solar radiation exhibited a widespread decreasing trend during the study period (Figure 2d), covering approximately 67.3% of the country, particularly in densely populated and industrialized areas like the North China Plain in the central region and the Sichuan Basin in the southwest. Despite the general decline in radiation, the robust growth of GPP underscores the dominant role of hydrothermal factors in driving the productivity of China's ecosystems at present.

To diminish the interaction effects among climatic factors, this study employed partial correlation analysis to reveal the response of GPP to precipitation, temperature, and radiation. The resulting spatial patterns exhibit significant heterogeneity (Figure 3). The relationship between GPP and precipitation shows a distinct north-south differentiation. In the northern regions, particularly in the semi-arid and semi-humid areas of eastern Inner Mongolia, the North China Plain, and the Loess Plateau, a widespread and significant positive correlation is observed (red areas). In contrast, GPP and precipitation show a significant negative correlation (blue areas) mainly in the southern China.

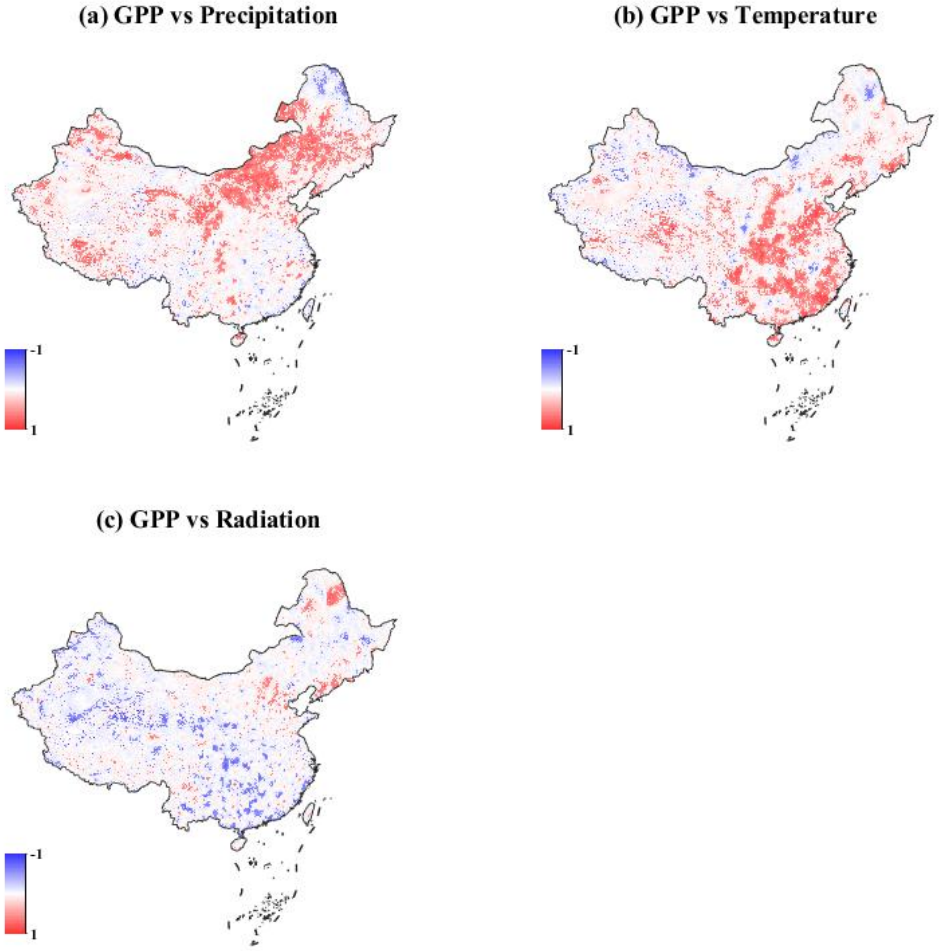

Figure 3. The partial correlation coefficients between GPP and climate factors including precipitation, temperature, and solar radiation.

© 2025 by the author(s). Distributed under a Creative Commons CC BY license.

Preprints.org (www.preprints.org) | NOT PEER-REVIEWED | Posted: 12 February 2026 doi:10.20944/preprints202602.1018.v1

The relationship between GPP and temperature is predominantly positive across vast areas of China. This is particularly evident in the eastern monsoon region, spanning from the northeast to the southeast, where temperature serves as a critical factor promoting vegetation productivity. Areas of negative correlation are more scattered, mainly appearing in parts of the arid zones and on the margins of the Qinghai-Tibet Plateau, where warming may exacerbate water stress and thus negatively impact GPP. The relationship between GPP and solar radiation presents a pattern contrary to the other two factors. A widespread negative correlation is found in the humid regions of southeastern China and in most of the arid northwest. Positive correlations are only observed in parts of the northeast and North China.

Table 2 reveals that the relationship between GPP and climatic factors exhibits significant heterogeneity across different ecosystem types and temporal scales. At the annual scale, the dominant climatic limiting factors for different ecosystems are clearly differentiated. Grassland and cropland are typical water-limited ecosystems, with the partial correlation of their annual GPP changes with precipitation (grassland r=0.58, cropland r=0.47) being much higher than that with temperature. In contrast, forests and shrublands are temperature-limited ecosystems, with their GPP being more sensitive to temperature (forest r=0.51, shrubland r=0.53) and relatively less affected by precipitation. Solar radiation generally exerts an inhibitory effect on GPP at the annual scale, particularly in grassland ecosystems (r=-0.35). Seasonal dynamics further reveal the complexity of climatic factor influences. Spring green-up is primarily driven by temperature (e.g., shrubland spring temperature r=0.67); in summer, intense solar radiation becomes a widespread inhibitory factor (national r=-0.53); and in autumn, the combined effect of temperature (e.g., shrubland autumn temperature r=0.81) and moisture (e.g., grassland autumn precipitation r=0.63) determines productivity at the end of the growing season.

Table 2. The partial correlation coefficient between GPP and climate factors under different land types.

Time scale	Climate Factor	China	Cropland	Forest	Shrubland	Grassland
Annual	PREC	0.70 ± 0.03	0.47 ± 0.06	0.34 ± 0.07	0.46 ± 0.06	0.58 ± 0.03
	TEMP	0.25 ± 0.08	0.25 ± 0.09	0.51 ± 0.09	0.53 ± 0.09	0.20 ± 0.07
	RAD	-0.40 ± 0.08	-0.15 ± 0.07	-0.06 ± 0.06	-0.05 ± 0.12	-0.35 ± 0.04
Monthly	PREC	0.28±0.15	0.16±0.15	0.16±0.14	0.23±0.11	0.31±0.15
	TEMP	0.42±0.19	0.36±0.25	0.47±0.23	0.58±0.28	0.20±0.14
	RAD	-0.11±0.26	-0.02±0.24	0.06±0.19	0.03±0.25	-0.11±0.21
Spring	PREC	0.41±0.06	0.03±0.08	0.20±0.07	0.31±0.10	0.31±0.05
	TEMP	0.29±0.04	0.50±0.05	0.63±0.05	0.67±0.07	0.25±0.06
	RAD	-0.23±0.05	-0.21±0.08	-0.11±0.06	-0.19±0.09	-0.14±0.06
Summer	PREC	0.22±0.08	0.19±0.06	-0.02±0.05	0.26±0.06	0.27±0.09
	TEMP	0.09±0.07	-0.10±0.09	0.16±0.08	0.10±0.11	0.13±0.07
	RAD	-0.53±0.07	-0.28±0.10	-0.18±0.06	-0.14±0.10	-0.38±0.07
Autumn	PREC	0.57±0.06	0.33±0.10	0.28±0.05	0.27±0.10	0.63±0.04
	TEMP	0.54±0.07	0.46±0.08	0.68±0.06	0.81±0.04	0.36±0.08
	RAD	-0.03±0.09	0.11±0.10	0.18±0.07	0.22±0.13	-0.14±0.09
Winter	PREC	0.29±0.09	0.17±0.09	0.17±0.10	0.33±0.14	0.30±0.07
	TEMP	0.48±0.05	0.42±0.07	0.44±0.07	0.68±0.07	0.30±0.03
	RAD	0.03±0.05	0.18±0.07	0.19±0.06	0.37±0.11	-0.30±0.05

The sensitivity of vegetation GPP to climatic factors shows a significant spatial differentiation across China (Figure 4). The response of GPP to changes in precipitation and temperature is predominantly positive, indicating that in most areas, improvements in hydrothermal conditions directly promote vegetation growth. The response of GPP to precipitation (Figure 4a) is mainly positive, especially in the semi-arid and arid regions of northern and western China. Strong positive sensitivity (deep red areas) is concentrated in the Northeast Plain, North China Plain, Loess Plateau, and eastern Inner Mongolia. Negative sensitivity appears on the edge of the Tarim Basin, in the

© 2025 by the author(s). Distributed under a Creative Commons CC BY license.

Preprints.org (www.preprints.org) | NOT PEER-REVIEWED | Posted: 12 February 2026 doi:10.20944/preprints202602.1018.v1

Sichuan Basin, and in southeastern coastal areas such as Fujian and Guangdong provinces. The positive sensitivity of GPP to temperature (Figure 4b) covers a vast area from the northeast to the southwest. Areas of negative sensitivity are more concentrated and significant mainly on the southern edge of the Qinghai-Tibet Plateau, the Yunnan-Guizhou Plateau, the southern China coast, and in some forest areas in the northeast. Unlike hydrothermal factors, the response of GPP to solar radiation (Figure 4c) displays a distinctly different spatial pattern. Negative sensitivity dominates the eastern monsoon region of China, from the Northeast Plain to the middle and lower reaches of the Yangtze River and South China. This suggests that in these areas with relatively favorable hydrothermal conditions, increased radiation is not the main driver of vegetation productivity and may even have an inhibitory effect in synergy with other environmental stresses (such as high temperature and drought). However, in low-energy areas such as the Qinghai-Tibet Plateau, the Tianshan Mountains, and other high-altitude mountain ranges, GPP shows a clear positive sensitivity to radiation.

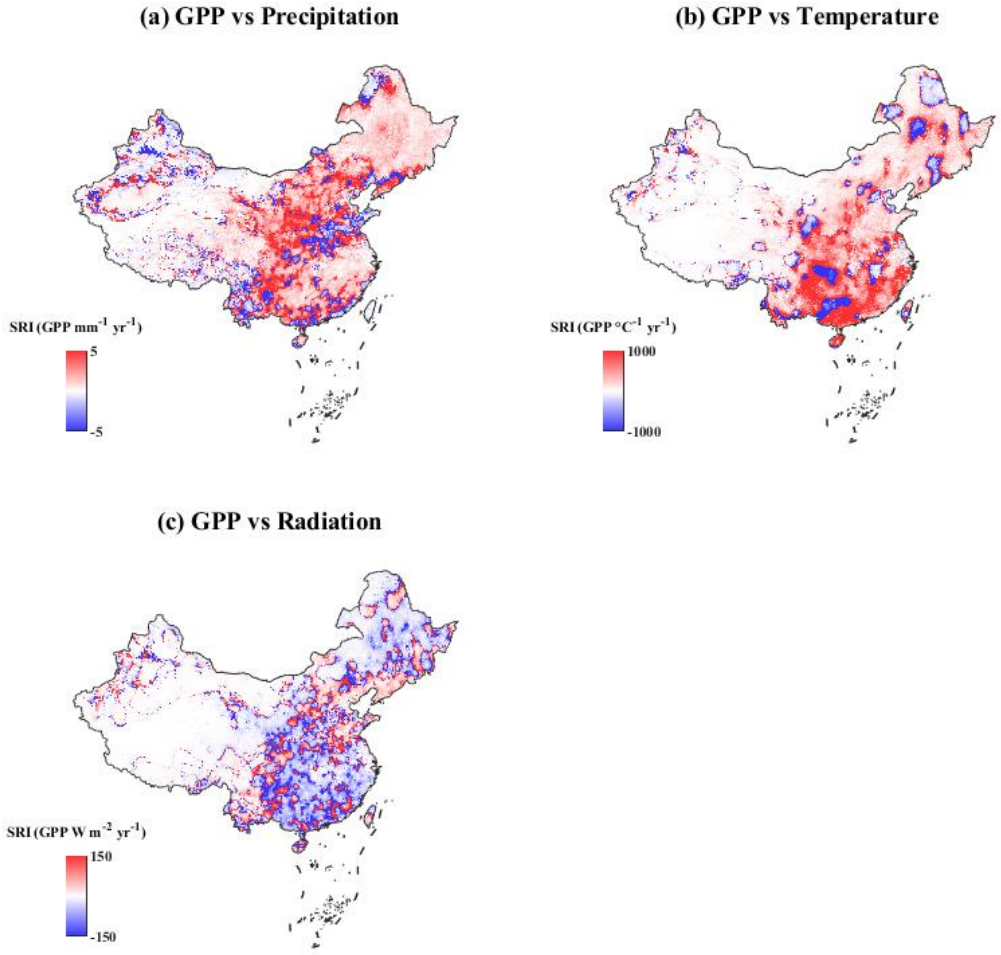

Figure 4. Spatial distribution of the sensitivity response index (SRI) of GPP to climatic factors across China at the annual scale during 2001–2020.

3.2. Divergent Effects of Topographic Conditions on GPP-Climate Relationships

The regulatory effect of the altitudinal gradient on GPP is most significant among all topographic factors. In terms of multi-year average distribution (Figure 5a), GPP exhibits a complex unimodal skewed distribution with increasing altitude, reaching a first peak at approximately 500 meters, followed by another high-value zone around 2500 meters, after which it declines with further increases in altitude. Above 4500 meters, GPP is extremely low. The change rate of GPP also shows clear vertical differentiation (Figure 5d). The strongest growth trend is concentrated in the low-to-

© 2025 by the author(s). Distributed under a Creative Commons CC BY license.

Preprints.org (www.preprints.org) | NOT PEER-REVIEWED | Posted: 12 February 2026 doi:10.20944/preprints202602.1018.v1

mid altitudes of 1000-2000 meters, then gradually weakens with increasing altitude, stabilizes around 4500 meters, and turns into negative rate at higher altitudes. This clearly indicates the presence of strong low-temperature limitations at high altitudes, presenting a threshold for vegetation growth. Slope primarily regulates GPP by affecting soil and water conditions in principle. The multi-year average GPP shows a trend of first increasing and then decreasing with increasing slope, reaching its maxima on gentle slopes of 10-15° (Figure 5b). Similarly, the interannual growth trend of GPP is most significant on gentle slopes of 5-10°, and the rate of vegetation improvement continuously decreases as the slope becomes steeper. In contrast, the influence of aspect is relatively weak. GPP on semi-sunny slopes (e.g., southeast and southwest) and west-facing slopes is slightly higher than that of north and northeast-facing slopes (Figure 5c). GPP change rate is characterized as consistent and positive (Figure 5f), showing the universality of the vegetation greening trend over the past two decades.

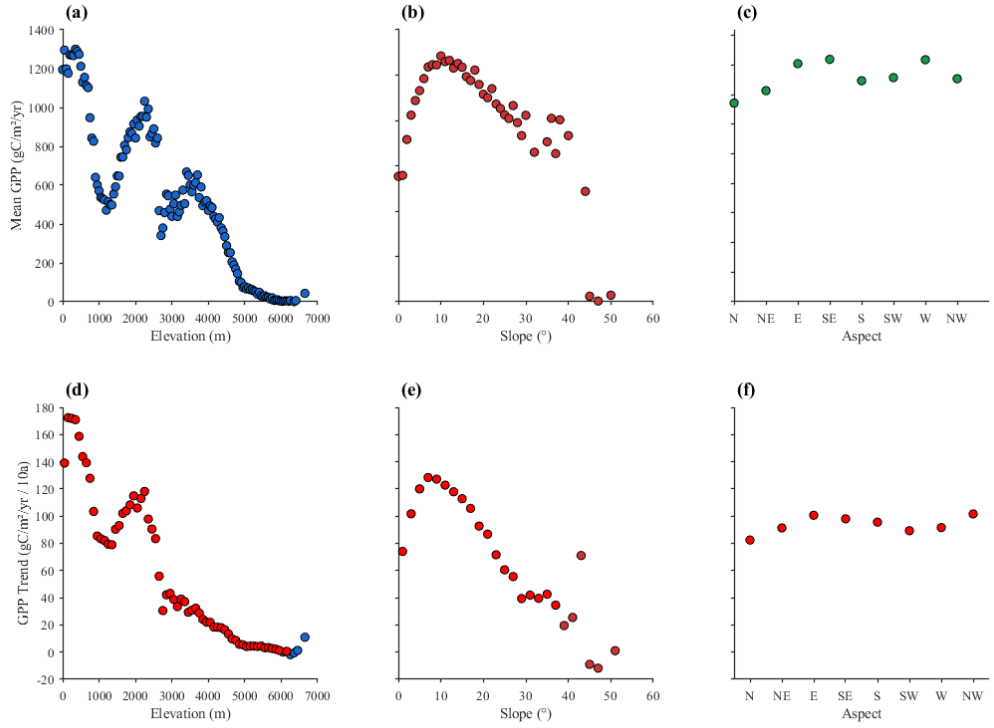

Figure 5. Distribution of interannual GPP variation across different altitudes, slopes, and aspects.

To reveal the effect of terrain on the GPP-climate relationship, we analyzed the partial correlations between GPP and major climatic factors across different terrain gradients (Figure 6). The analysis indicates that topographical factors significantly regulate the response of GPP to key climatic drivers. First, the altitudinal gradient reveals a clear transition of the dominant climatic limiting factors. In areas below 2000 meters, GPP shows a strong positive correlation with precipitation. As altitude increases, the influence of precipitation gradually diminishes, while the promotive effect of temperature becomes significantly enhanced, becoming the primary positive driver in high-altitude regions of 3000-4000 meters. In contrast, the effect of solar radiation is more complex, showing a weak positive correlation at very low altitudes but rapidly transitioning to the opposite with increasing altitude. Changes in slope also alter the relative importance of climatic factors. On gentle slopes of 0-5°, GPP is co-dominated by precipitation (positive) and radiation (negative). As the slope increases, the influence of both precipitation and radiation tends to weaken, while the positive effect of temperature becomes more prominent, with its positive correlation peaking on steep slopes of 20-30°. This may be related to better drainage conditions and heat redistribution on steeper slopes.

© 2025 by the author(s). Distributed under a Creative Commons CC BY license.

Preprints.org (www.preprints.org) | NOT PEER-REVIEWED | Posted: 12 February 2026 doi:10.20944/preprints202602.1018.v1

Across different aspects, the influence of climatic factors shows a high degree of consistency. Precipitation (strong positive correlation) and solar radiation (strong negative correlation) are consistently the dominant drivers of GPP change, with their partial correlation coefficients being much higher than that of temperature.

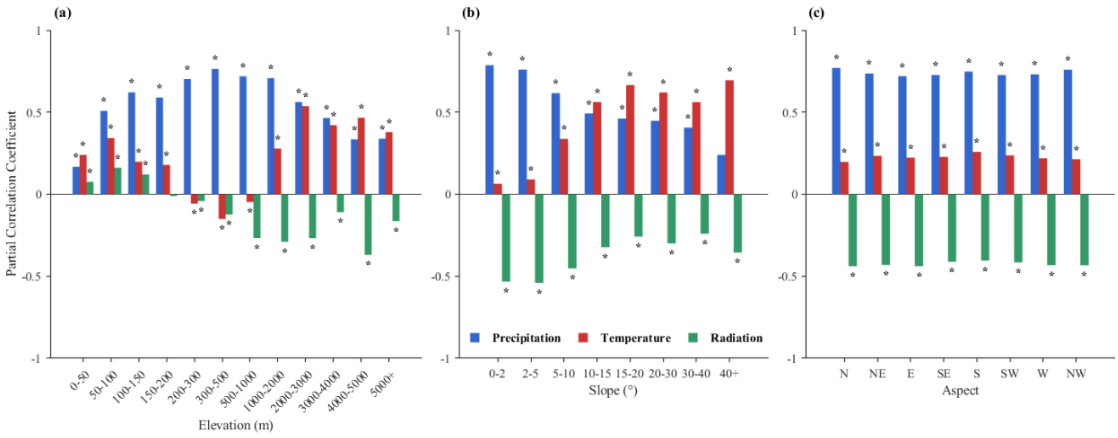

Figure 6. Partial correlations between GPP and climatic factors along terrain gradients. The asterisks (*) indicate that the correlation is statistically significant at the $p<0.05$ level.

To investigate how terrain gradients modulate the sensitivity of GPP to climate change, this study calculated the response slopes of GPP to three key climatic factors under different terrain groupings (Figure 7). The influence of the altitudinal gradient is the most complex and prominent. The sensitivity of GPP to precipitation exhibits a clear "inverted U-shaped" pattern with increasing altitude, peaking in the mid-altitude range of 1000-2000 meters. This indicates that ecosystems in this region are most sensitive to changes in moisture; at higher or lower altitudes, the sensitivity decreases. Conversely, the sensitivity of GPP to temperature continuously decreases with increasing altitude. For radiation, its inhibitory effect on GPP (negative sensitivity) is also strongest in the mid-altitude (500-2000 meters) region. Slope also significantly modulates the climate sensitivity of GPP. The sensitivity of GPP to temperature shows a trend of first increasing and then decreasing with an increase in slope, peaking at a moderate slope of 15-20°, suggesting that moderately inclined terrain may create more optimal conditions for hydrothermal redistribution, hence amplifying vegetation's response to temperature changes. The sensitivity of GPP to precipitation monotonically decreases with increasing slope, possibly because on steeper slopes increased precipitation is more likely to be lost as runoff, reducing its effectiveness for vegetation growth. In comparison, the regulatory effect of different aspects on climate sensitivity is relatively weak, with no significant differences among various aspects.

To assess the relative importance of different climatic factors on GPP, we calculated standardized sensitivity coefficients (Figure 8). This method eliminates differences in variable value ranges and units, allowing for a direct comparison of the influence of each climatic driver. Precipitation is the most dominant positive factor driving GPP changes. In all terrain groupings, precipitation exhibits the strongest positive sensitivity (standardized sensitivity coefficients ranging from 0.723 to 0.791), which is most strongly modulated by aspects. Temperature is also an important positive driver of GPP, but its relative importance is secondary to precipitation. The standardized sensitivity coefficients for temperature range from 0.536 to 0.726, with slope being its most significant modulating factor. In contrast, solar radiation shows an inhibitory effect on GPP. Its standardized sensitivity coefficients are all negative, and this negative effect is most pronounced under the slope group (-0.690).

© 2025 by the author(s). Distributed under a Creative Commons CC BY license.

Preprints.org (www.preprints.org) | NOT PEER-REVIEWED | Posted: 12 February 2026 doi:10.20944/preprints202602.1018.v1

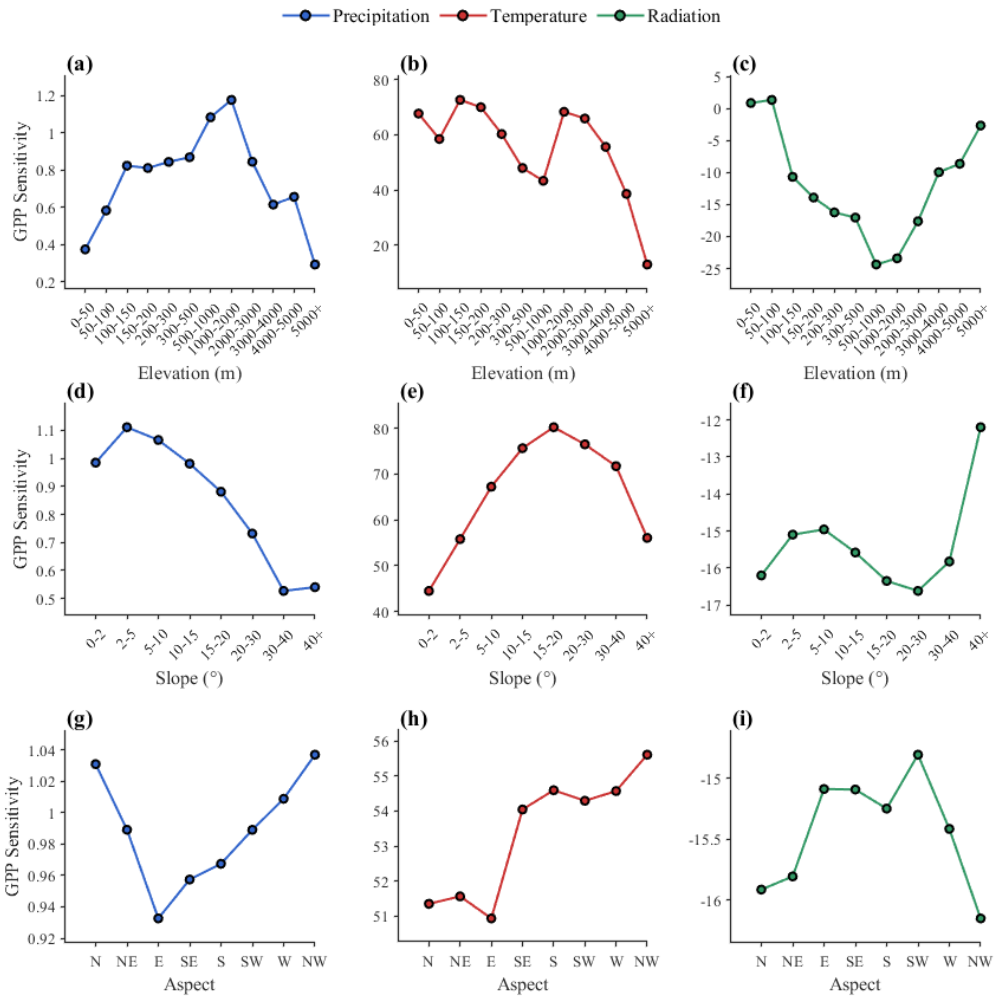

Figure 7. Sensitivity of GPP to climatic factors along terrain gradients.

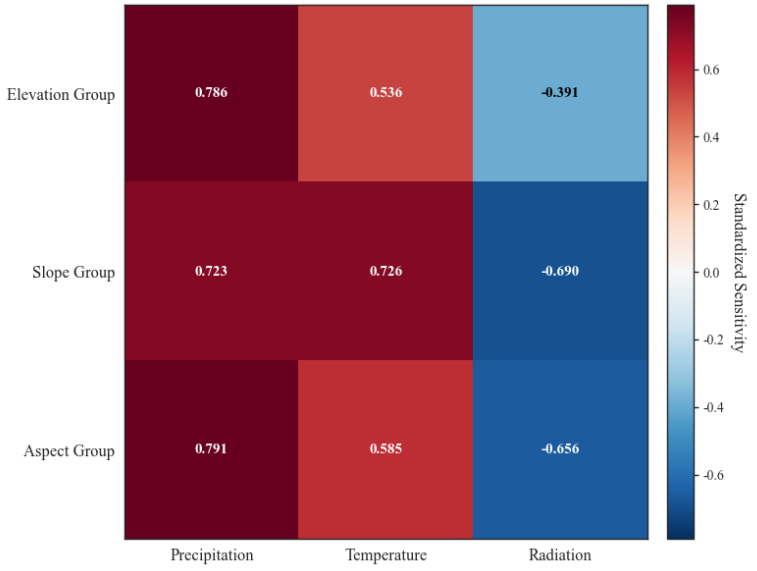

Figure 8. Standardized sensitivity of GPP to climate variables by topographic groups at the annual scale.

© 2025 by the author(s). Distributed under a Creative Commons CC BY license.

Preprints.org (www.preprints.org) | NOT PEER-REVIEWED | Posted: 12 February 2026 doi:10.20944/preprints202602.1018.v1

3.3. Cascading Effects of Climate and Topography on GPP Among Land Use Types

To reveal the complex causal pathways of terrain factors and climate variables on GPP, we constructed a structural equation model (SEM). The results clarify the direct driving effects of climatic factors on GPP, as well as how terrain factors indirectly influence GPP by modulating climate (Figure 9). In terms of direct effects, precipitation is the strongest climatic factor promoting GPP with a path coefficient of 0.605, followed by temperature, while solar radiation exhibits an inhibitory effect. Regarding indirect effects, altitude has a total path coefficient of -0.608, compared to 0.369 from slope on GPP. In contrast, the coefficient for aspect and GPP is only 0.012, indicating that aspect is not a dominant terrain factor. Overall, terrain as a composite variable has a net negative total effect of -0.227 on GPP, with the indirect regulatory role of altitude being dominant.

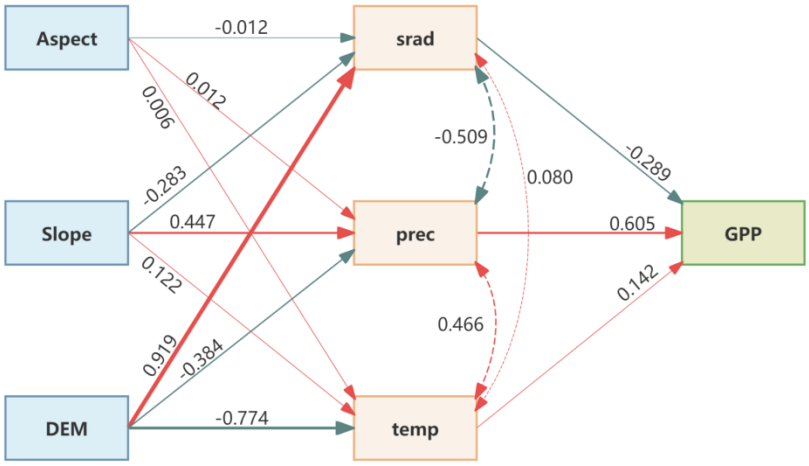

Figure 9. Diagram of structural equation model results between topographic and climatic factors and GPP over the entire China.

We further investigate the impacts of climate and topography on GPP for cropland, forest, shrubland, and grassland (Figure 10). The results categorize the four ecosystems into two distinct types. Cropland and grassland are characterized as water-limited ecosystems. In these two types, the direct promoting effect of precipitation on GPP is the strongest with a path coefficient for cropland and grassland of 0.697 and 0.556, respectively. In contrast, forests and shrublands are characterized as hydrothermal co-limited ecosystems. In these ecosystems, both precipitation and temperature show significant and comparably strong positive direct effects on GPP, indicating that their productivity requires the co-driving of both water and heat. Secondly, the SEM results also reveal that the regulatory role of terrain factors differs among different ecosystems. Slope is the key terrain factor affecting GPP in cropland and grassland, primarily by significantly influencing precipitation distribution (path coefficient of 0.415 and 0.404 for cropland and grassland, respectively), indirectly affecting GPP.

To quantitatively assess the explanatory power of different driving factors on the spatial differentiation of GPP, we employed the Geodetector model. The factor detector results (Figure 11) reveal the relative importance of each driver. Precipitation is the primary driving factor explaining the spatial pattern of GPP, with a q-statistic as high as 0.725, far exceeding all other factors. Among the terrain factors, altitude (q=0.287) has a moderate level of explanatory power, while the direct influence of slope and aspect is relatively weak. Meanwhile, the interaction detector results show that the interactions between all pairs of factors are either bivariate enhancement or non-linear enhancement. Among them, the interaction between precipitation and altitude is the strongest, with an interaction q-value reaching 0.849. This indicates that the effect of precipitation on vegetation GPP is significantly amplified across different altitudinal gradients.

© 2025 by the author(s). Distributed under a Creative Commons CC BY license.

Preprints.org (www.preprints.org) | NOT PEER-REVIEWED | Posted: 12 February 2026 doi:10.20944/preprints202602.1018.v1

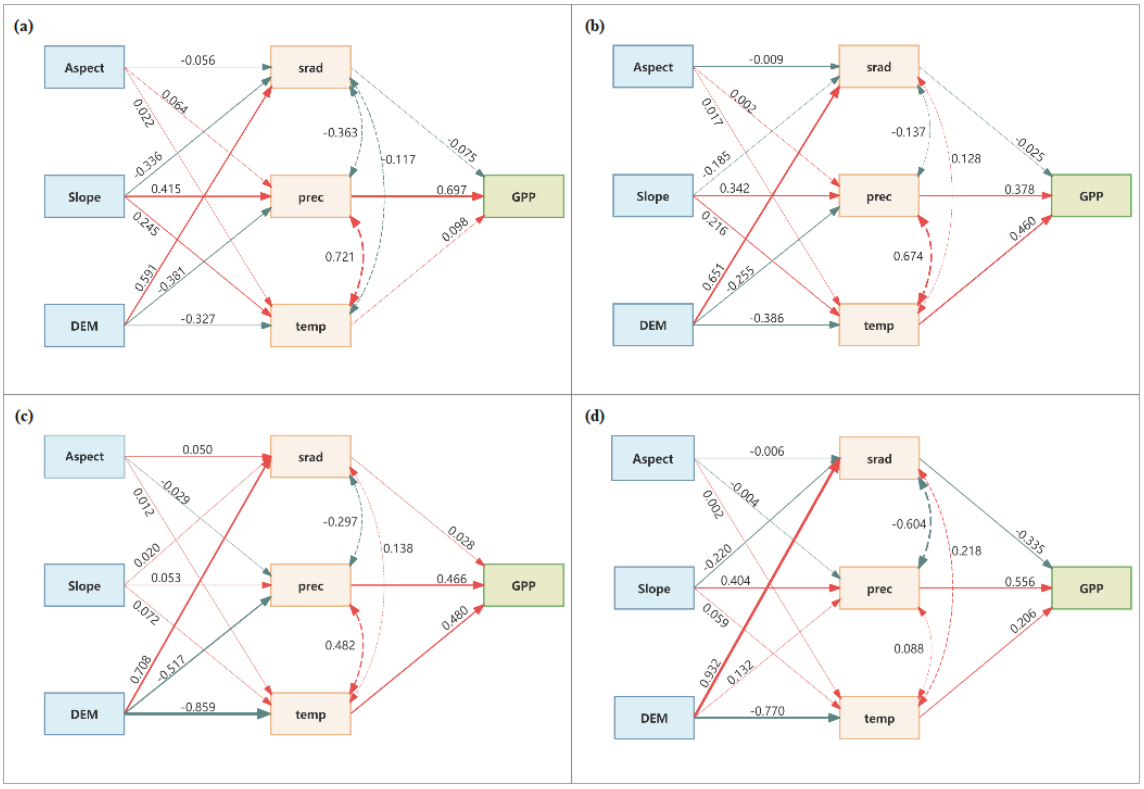

Figure 10. Diagram of structural equation model results between topographic and climatic factors and GPP over four dominant land use type groups.

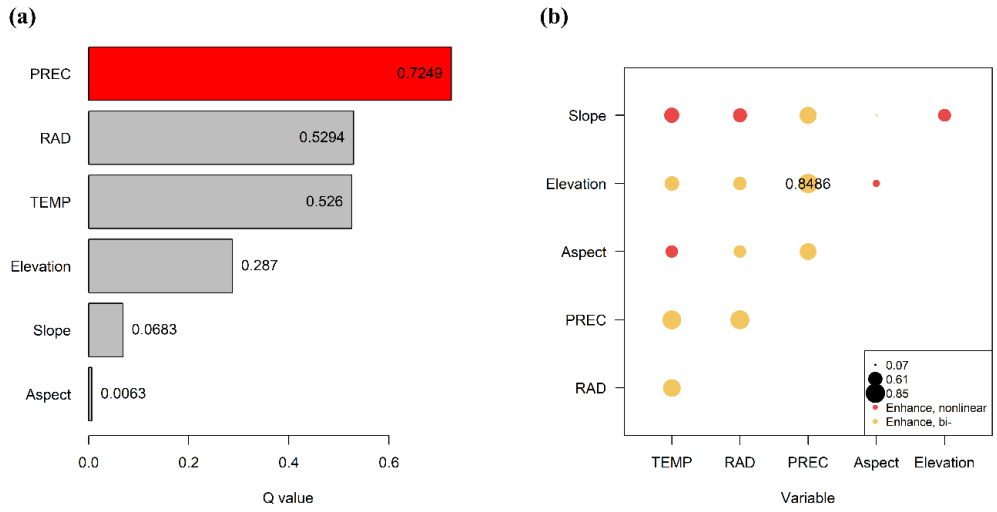

Figure 11. Driving factors for GPP spatial heterogeneity identified by the Geodetector model.

To explore the non-linear response relationships of GPP to key climatic factors and to determine their thresholds, this study utilized a Generalized Additive Model (GAM). The results clearly reveal that the response of GPP to each climatic factor exhibits distinct threshold effects (Figure 12). First, the response of GPP to temperature shows a typical pattern of initial promotion followed by inhibition. In the cold regions, temperature is the main limiting factor, and GPP increases significantly with rising temperature. When the temperature exceeds a saturation point of approximately 17.4°C, the growth trend of GPP slows down markedly and stabilizes afterwards. This suggests that excessively high temperatures can trigger stress-induced physiological responses such as stomatal closure, hence offsetting the benefits of further warming. Second, the response of GPP to precipitation demonstrates a pattern of rapid growth followed by saturation. When precipitation is low, moisture

© 2025 by the author(s). Distributed under a Creative Commons CC BY license.

Preprints.org (www.preprints.org) | NOT PEER-REVIEWED | Posted: 12 February 2026 doi:10.20944/preprints202602.1018.v1

is the decisive factor limiting vegetation growth, and GPP increases rapidly with increasing precipitation. When precipitation reaches a saturation threshold of about 1974 mm, the GAM response curve flattens, indicating that moisture is no longer the primary limiting factor, and further increases in precipitation have a very limited effect on GPP. The response of GPP to solar radiation is more complex, showing a trend of slight initial growth followed by a continuous decline. At low radiation levels, GPP slightly increases with enhanced radiation. However, when the radiation intensity exceeds about 101 W/m², GPP begins to show a clear downward trend. This may be because high radiation is often accompanied by high temperatures and strong evapotranspiration, causing photoinhibition and water stress on vegetation, which in turn has a negative impact on photosynthesis.

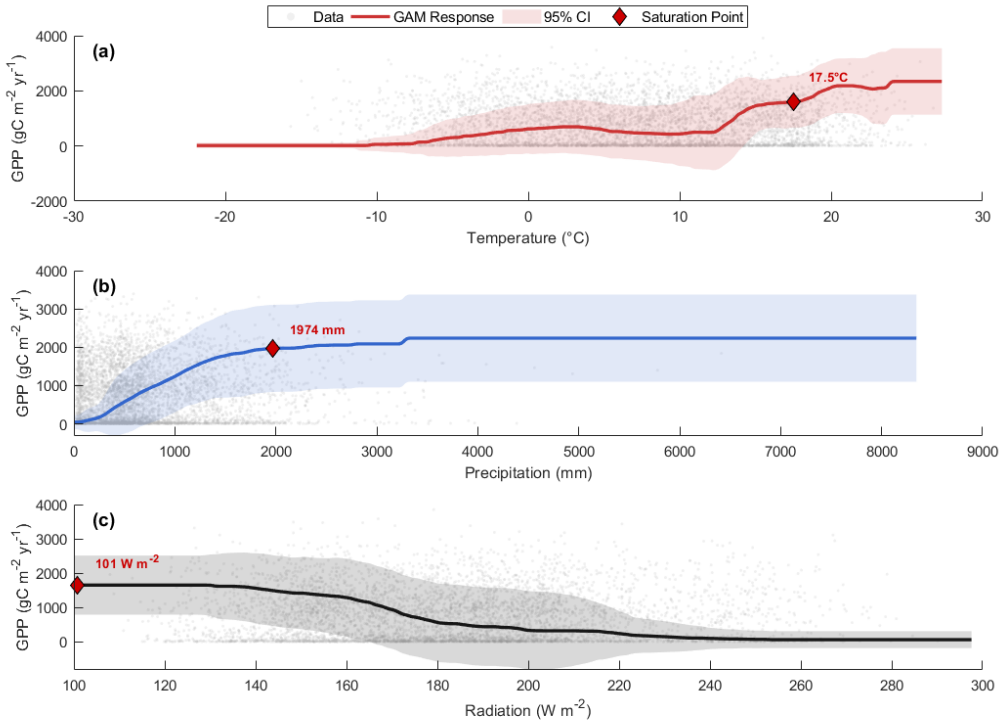

Figure 12. GAM-derived response curves revealing climatic thresholds for GPP.

4. Discussion

4.1. Spatiotemporal Changes of GPP and the Climatic Drivers

From 2001 to 2020, China's terrestrial ecosystems exhibited a significant and widespread increase in GPP, with 79.3% of the country showing an upward trend. This greening pattern, spatially stronger in the eastern and southern regions, aligns with the widely observed global greening phenomenon [51,52]. This enhanced productivity coincided with nationwide increases in precipitation and temperature, underscoring the dominant role of improved hydrothermal conditions [53]. Spatially, the most significant GPP growth occurred in the humid forests and croplands of the southeast, whereas degradation in central Inner Mongolia and the Loess Plateau reflected the vulnerability of arid regions to soil moisture deficits [54]. Notably, this robust national-scale growth occurred despite a widespread decrease in solar radiation attributed to anthropogenic aerosols [55], suggesting that high radiation, which is often coupled with heat and water stress, may exert long-term inhibitory effects.

© 2025 by the author(s). Distributed under a Creative Commons CC BY license.

Preprints.org (www.preprints.org) | NOT PEER-REVIEWED | Posted: 12 February 2026 doi:10.20944/preprints202602.1018.v1

Although climate change drives productivity [56], the complex multicollinearity among drivers [23,57] necessitates analysis by land use types. A distinct north-south divergence exists in the GPP-precipitation relationship. In the water-scarce northern regions, grasslands and croplands are unequivocally water-limited; thus, precipitation directly alleviates water stress and boosts productivity [58]. Conversely, a significant negative correlation emerges in the humid southern regions and high-latitude forests (Figure 3). In such areas, excessive precipitation is often associated with increased cloud cover (limiting light) or soil waterlogging (inducing anoxia), which inhibits photosynthesis [59,60]. This indicates that once rainfall exceeds a certain threshold [61], it causes significant inhibition to vegetation growth. Temperature, in contrast, exhibits widespread positive sensitivity (Figure 4b), particularly in forests and shrublands. In these non-water-restricted regions, warming likely enhances GPP by extending the growing season and increasing enzymatic activity [62]. Solar radiation reveals a widespread inhibitory effect. In the humid southeast, high radiation increases vapor pressure deficit (VPD) and induces stomatal closure; in the arid northwest, it serves as a proxy for clear skies and precipitation deficit, exacerbating water stress [55].

4.2. The Regulatory Effect of Terrain Conditions on GPP-Climate Relationships

Topography exerts a profound regulatory effect on GPP dynamics. The altitudinal gradient is the most significant factor. GPP peaks around 500m in the productive eastern lowlands, but declines sharply above 4500m due to extreme low-temperature constraints [63], and permafrost-altered hydrology [64]. The strongest growth trend is concentrated in the mid-altitudes (1000–2000m). This region represents an ecological "sweet spot" [65]: it is high enough to avoid intensive human disturbance, yet low enough that regional warming alleviates thermal stress. The elevation-dependent warming likely extends the growing season, driving the rapid productivity increase. Conversely, the trend turns negative at extreme altitudes (>4500m), confirming that these energy-limited ecosystems are at a critical threshold where low-temperature limitations become prominent.

Slope gradients introduce a secondary modulation by controlling local hydrology. The observed peak in GPP on gentle slopes (5–15°) represents an optimal balance. Steeper slopes (>15-20°) clearly inhibit GPP, a mechanism attributed to rapid surface runoff which reduces effective infiltration and soil development [66]. Conversely, very gentle slopes (0-5°) can also be suboptimal due to potential waterlogging and root hypoxia in poorly-drained lowlands [67]. While aspect creates important microclimatic gradients [68], its influence remains relatively weak at this national scale compared to altitude and slope.

Crucially, topography fundamentally alters climatic constraints. The shift from precipitation-dominated systems at low elevations (<2000 m) to temperature-dominated systems at high elevations (>3000–4000 m) is a classic demonstration of eco-physiological resource limitation theory [69]. As elevation increases, the adiabatic lapse rate creates an energy-limited environment where cold temperatures override the influence of precipitation. Our findings show that carbon uptake sensitivity to temperature is highest in high-elevation environments [70]. A key observation is the non-linear, inverted U-shaped pattern of GPP sensitivity to precipitation [71], which peaks in the mid-altitude range (1000–2000 m). This identifies the mid-altitude band as a critical ecological transition zone. The underlying mechanism is that these ecosystems are uniquely poised at a biophysical crossover point: they are coordinated by both water and energy, rather than being chronically limited by just one [72]. Consequently, a given increment of precipitation yields the maximum positive GPP response here, as there is sufficient energy to utilize the extra water. Thus, these ecosystems act as hotspots of climatic responsiveness [73].This analysis also resolves a discrepancy in our temperature sensitivity findings: while temperature's relative importance increases with altitude (Figure 6), its absolute sensitivity decreases (Figure 7). This demonstrates that at extreme high altitudes (>4000 m), GPP is so severely constrained by low energy that it becomes limited by tissue formation rather than photosynthetic production [74]. Even if temperature is the primary driver, the low thermal conditions restrict the plant community's absolute capacity to add new biomass. Finally, the finding that GPP sensitivity to precipitation monotonically decreases with

© 2025 by the author(s). Distributed under a Creative Commons CC BY license.

Preprints.org (www.preprints.org) | NOT PEER-REVIEWED | Posted: 12 February 2026 doi:10.20944/preprints202602.1018.v1

increasing slope (Figure 7b) confirms that on steep terrain, runoff losses decouple vegetation growth from precipitation inputs [75].

SEM and Geodetector analyses clarified this causal architecture. Precipitation is identified as the single most dominant factor (path 0.605), while altitude exerts the strongest negative total effect (-0.608) by governing local thermal-hydrological regimes [76]. The interaction between precipitation and elevation yields the highest explanatory power, confirming that moisture effects are contingent upon elevation [57]. Land-use-specific SEMs reveal distinct strategies: Croplands and grasslands are strongly water-limited, with productivity directly coupled to short-term precipitation [77]. In contrast, forests and shrublands function as hydrothermal co-limited ecosystems [78], using deeper roots to buffer against variability.

4.3. Quantification of Nonlinear Thresholds and the Ecological Implications

The quantification of climatic thresholds via the GAM analysis reveals that the response of China's terrestrial ecosystems to climate change is fundamentally non-linear. These findings resonate with emerging global evidence suggesting that terrestrial carbon sinks are transitioning from a regime dominated by simple linear drivers to one increasingly constrained by physiological limits and climatic extremes [79]. Our study identifies a thermal turning point for GPP at approximately 17.4°C. This threshold aligns with global observations of temperature optima for temperate ecosystems, which are significantly lower than those in tropical forests [80]. The mechanism behind this saturation is likely driven by atmospheric aridity. As demonstrated by Yuan et al. [81], rising temperatures are inextricably linked to exponential increases in Vapor Pressure Deficit (VPD). High VPD triggers rapid stomatal closure to prevent hydraulic failure, a physiological defense that restricts carbon uptake even when soil moisture is sufficient [82]. Thus, the 17.4°C threshold marks the point where VPD-induced stress overrides the kinetic benefits of warming. The precipitation saturation threshold of ~1974 mm provides region-specific evidence for the water-energy trade-off. While water is the primary driver in arid zones, Humphrey et al. [83] highlighted that in humid regions land carbon uptake becomes decoupled from soil moisture and increasingly limited by energy availability. We observed that GPP gains stagnate above ~2000 mm. This saturation effect is consistent with the increasing global water constraint on vegetation growth noted by Jiao et al. [84], suggesting that excessive water inputs may no longer enhance productivity due to associated limitations such as nutrient leaching or reduced radiation. The observation that solar radiation inhibits GPP above ~101 W/m² challenges the simplistic view of light limitation. This aligns with the findings of Knohl and Baldocchi [85], who demonstrated that canopy light use efficiency declines significantly under clear-sky conditions dominated by direct beam radiation. They attributed this to the fact that high direct irradiance rapidly saturates photosynthesis in the upper canopy leaves, whereas diffuse radiation penetrates deeper into the canopy to illuminate shaded leaves, thereby maintaining higher overall carbon uptake rates. High direct irradiance often heats leaves beyond their thermal optimum and exacerbates transpiration stress [86]. Thus, our threshold marks the transition where radiative heat stress overrides the benefits of photon availability. The existence of these sharp thresholds has profound implications for Earth System Models (ESMs). Current models often underestimate the impacts of climate extremes on the carbon cycle [87]. Failing to parameterize these saturation points (e.g., the VPD constraint identified by Yuan et al. [81]) risks overestimating future land carbon sinks. Consequently, regional ecological management must recognize that afforestation efforts in areas surpassing these climatic thresholds may yield diminishing returns as ecosystems approach their physiological limits.

5. Conclusions

This study investigated the spatiotemporal dynamics of GPP across China's terrestrial ecosystems from 2001 to 2020, confirming the dominant driving role of precipitation and the significant cascading effects of topography and climate. Beyond verifying a widespread greening trend, our core finding reveals that topography is not a static background but a dynamic regulator

© 2025 by the author(s). Distributed under a Creative Commons CC BY license.

Preprints.org (www.preprints.org) | NOT PEER-REVIEWED | Posted: 12 February 2026 doi:10.20944/preprints202602.1018.v1

that reallocates hydrothermal resources. This regulation shifts ecosystem constraints from water limitation at low altitudes to energy limitation at high altitudes, establishing mid-altitude regions as a unique ecological "sweet spot". Crucially, we identified non-linear physiological thresholds using the GAM method, specifically ~17.4°C for temperature, ~1974 mm for precipitation, and ~101 W/m² for solar radiation, which challenge conventional linear assumptions. These results serve as a warning that under future climate extremes, continuous warming and wetting in many parts of the world may eventually exceed physiological limits, leading to saturation or even inhibition rather than promotion of vegetation growth and carbon assimilation. Collectively, these findings provide a parameterized mechanistic understanding of the non-linear responses of terrestrial carbon sinks, underscoring the necessity of incorporating topographic modulation and climatic tipping points into future Earth system models and ecological management policies.

Author Contributions: Conceptualization, validation, resources, supervision, funding acquisition, project administration, writing—review and editing, Hailong Wang; methodology, formal analysis, investigation, data curation, visualization, writing—original draft preparation, Minqian He. All authors have read and agreed to the published version of the manuscript.

Funding: This study was supported by the National Key Research and Development Program, China [2021YFC3200202], the National Natural Science Foundation of China [42171020], and the Guangdong Provincial Department of Science and Technology, China [2019ZT08G090].

Data Availability Statement: The datasets supporting the findings of this study are openly available in the following repositories: GPP data: The Global 0.05-degree GOSIF GPP product is available from the authors of Li and Xiao (2019) and related publications. The China Meteorological Forcing Dataset (CMFD) is available at the National Tibetan Plateau Data Center: *https://www.tpdc.ac.cn*. The China Land Cover Dataset (CLCD) is available on Zenodo: *https://zenodo.org/records/8176941*. The SRTM Version 4 DEM is available from the CGIAR-CSI GeoPortal: *https://srtm.csi.cgiar.org*.

Conflicts of Interest: The authors declare no conflicts of interest. The funders had no role in the design of the study; in the collection, analyses, or interpretation of data; in the writing of the manuscript; or in the decision to publish the results.

References

1. Huang, H.; Xue, Y.; Chilukoti, N.; Liu, Y.; Chen, G.; Diallo, I. Assessing Global and Regional Effects of Reconstructed Land-Use and Land-Cover Change on Climate since 1950 Using a Coupled Land–Atmosphere–Ocean Model. **2020**, doi:10.1175/JCLI-D-20-0108.1.
2. Piao, S.; Cui, M.; Chen, A.; Wang, X.; Ciais, P.; Liu, J.; Tang, Y. Altitude and Temperature Dependence of Change in the Spring Vegetation Green-up Date from 1982 to 2006 in the Qinghai-Xizang Plateau. *Agricultural and Forest Meteorology* **2011**, *151*, 1599–1608, doi:10.1016/j.agrformet.2011.06.016.
3. Zhou, S.; Williams, A.P.; Lintner, B.R.; Berg, A.M.; Zhang, Y.; Keenan, T.F.; Cook, B.I.; Hagemann, S.; Seneviratne, S.I.; Gentine, P. Soil Moisture–Atmosphere Feedbacks Mitigate Declining Water Availability in Drylands. *Nat. Clim. Chang.* **2021**, *11*, 38–44, doi:10.1038/s41558-020-00945-z.
4. Beer, C.; Reichstein, M.; Tomelleri, E.; Ciais, P.; Jung, M.; Carvalhais, N.; Rödenbeck, C.; Arain, M.A.; Baldocchi, D.; Bonan, G.B.; et al. Terrestrial Gross Carbon Dioxide Uptake: Global Distribution and Covariation with Climate. *Science* **2010**, *329*, 834–838, doi:10.1126/science.1184984.
5. Xiahou, M.; Liu, Y.; Yang, T.; Shen, Z. Estimating Potential Vegetation Distribution and Restoration in a Biodiversity Hotspot Region under Future Climate Change. *J. Geogr. Sci.* **2024**, *34*, 2128–2144, doi:10.1007/s11442-024-2286-z.
6. Li, H.; He, Y.; Zhang, L.; Cao, S.; Sun, Q. Spatiotemporal Changes of Gross Primary Production in the Yellow River Basin of China under the Influence of Climate-Driven and Human-Activity. *Global Ecology and Conservation* **2023**, *46*, e02550, doi:10.1016/j.gecco.2023.e02550.

© 2025 by the author(s). Distributed under a Creative Commons CC BY license.

Preprints.org (www.preprints.org) | NOT PEER-REVIEWED | Posted: 12 February 2026 doi:10.20944/preprints202602.1018.v1

7. Wu, X.; Zhang, R.; Bento, V.A.; Leng, S.; Qi, J.; Zeng, J.; Wang, Q. The Effect of Drought on Vegetation Gross Primary Productivity under Different Vegetation Types across China from 2001 to 2020. *Remote Sensing* **2022**, *14*, 4658, doi:10.3390/rs14184658.
8. Lai, J.; Qi, S. Coupled Effects of Climate Change and Human Activities on Vegetation Dynamics in the Southwestern Alpine Canyon Region of China. *J. Mt. Sci.* **2024**, *21*, 3234–3248, doi:10.1007/s11629-024-9002-4.
9. Yao, Y.; Wang, X.; Li, Y.; Wang, T.; Shen, M.; Du, M.; He, H.; Li, Y.; Luo, W.; Ma, M.; et al. Spatiotemporal Pattern of Gross Primary Productivity and Its Covariation with Climate in China over the Last Thirty Years. *Global Change Biology* **2018**, *24*, 184–196, doi:10.1111/gcb.13830.
10. *IPCC, 2021*; IPCC, Zhai, P., Pirani, A., Connors, S.L., Péan, C., Berger, S., Caud, N., Chen, Y., Goldfarb, L., Gomis, M.I., Huang, M., Leitzell, K., Lonnoy, E., Matthews, J.B.R., Maycock, T.K., Waterfield, T., Yelekçi, Ö., Yu, R., Zhou, B., Eds.; Cambridge University Press: Cambridge, United Kingdom and New York, NY, USA, 2021;
11. Yang, X.; Liu, S.; Yang, T.; Xu, X.; Kang, C.; Tang, J.; Wei, H.; Ghebrezgabher, M.G.; Li, Z. Spatial-Temporal Dynamics of Desert Vegetation and Its Responses to Climatic Variations over the Last Three Decades: A Case Study of Hexi Region in Northwest China. *J. Arid Land* **2016**, *8*, 556–568, doi:10.1007/s40333-016-0046-3.
12. Gao, X.; Huang, X.; Lo, K.; Dang, Q.; Wen, R. Vegetation Responses to Climate Change in the Qilian Mountain Nature Reserve, Northwest China. *Global Ecology and Conservation* **2021**, *28*, e01698, doi:10.1016/j.gecco.2021.e01698.
13. Gao, B.; Liu, E.; Yang, Y.; Yang, M.; Yao, Y.; Guan, L.; Feng, Y. Quantitative Contributions of Climate Change and Human Activities to Vegetation Dynamics in the Zoige Plateau from 2001 to 2020. *J. Mt. Sci.* **2024**, *21*, 3031–3046, doi:10.1007/s11629-024-8720-y.
14. Peng, W.; Kuang, T.; Tao, S. Quantifying Influences of Natural Factors on Vegetation NDVI Changes Based on Geographical Detector in Sichuan, Western China. *Journal of Cleaner Production* **2019**, *233*, 353–367, doi:10.1016/j.jclepro.2019.05.355.
15. Xue, S.; Wu, G. Sensitivities of Vegetation Gross Primary Production to Precipitation Frequency in the Northern Hemisphere from 1982 to 2015. *Remote Sensing* **2024**, *16*, 21, doi:10.3390/rs16010021.
16. He, B.; Chen, A.; Jiang, W.; Chen, Z. The Response of Vegetation Growth to Shifts in Trend of Temperature in China. *J. Geogr. Sci.* **2017**, *27*, 801–816, doi:10.1007/s11442-017-1407-3.
17. Mercado, L.M.; Bellouin, N.; Sitch, S.; Boucher, O.; Huntingford, C.; Wild, M.; Cox, P.M. Impact of Changes in Diffuse Radiation on the Global Land Carbon Sink. *Nature* **2009**, *458*, 1014–1017, doi:10.1038/nature07949.
18. Du, G.; Yan, S.; Chen, H.; Yang, J.; Wen, Y. Intra-Annual Cumulative Effects and Mechanisms of Climatic Factors on Global Vegetation Biomes' Growth. *Remote Sensing* **2024**, *16*, 779, doi:10.3390/rs16050779.
19. Tuoku, L.; Wu, Z.; Men, B. Impacts of Climate Factors and Human Activities on NDVI Change in China. *Ecological Informatics* **2024**, *81*, 102555, doi:10.1016/j.ecoinf.2024.102555.
20. Ren, H.; Wen, Z.; Liu, Y.; Lin, Z.; Han, P.; Shi, H.; Wang, Z.; Su, T. Vegetation Response to Changes in Climate across Different Climate Zones in China. *Ecological Indicators* **2023**, *155*, 110932, doi:10.1016/j.ecolind.2023.110932.
21. Yan, T.; Kang, Y.; Xie, S.; Tao, C.; Li, L.; Li, X.; Wang, Q.; Zhang, Y. Differences in Growth Responses to Climate of Three Conifer Species in Lugu Lake of Northwestern Yunnan, Southwestern China. *Plants (Basel)* **2025**, *14*, 2508, doi:10.3390/plants14162508.
22. Zhang, Y.; Wang, Q.; Zhang, X.; Guo, Z.; Guo, X.; Ma, C.; Wei, B.; He, L. Pre-Season Precipitation and Temperature Have a Larger Influence on Vegetation Productivity than That of the Growing Season in the Agro-Pastoral Ecotone in Northern China. *Agriculture* **2025**, *15*, 219, doi:10.3390/agriculture15020219.
23. Quetin, G.R.; Swann, A.L.S. Empirically Derived Sensitivity of Vegetation to Climate across Global Gradients of Temperature and Precipitation. **2017**, doi:10.1175/JCLI-D-16-0829.1.
24. Zhao, W.; Hu, Z.; Guo, Q.; Wu, G.; Chen, R.; Li, S. Contributions of Climatic Factors to Interannual Variability of the Vegetation Index in Northern China Grasslands. **2020**, doi:10.1175/JCLI-D-18-0587.1.

© 2025 by the author(s). Distributed under a Creative Commons CC BY license.

Preprints.org (www.preprints.org) | NOT PEER-REVIEWED | Posted: 12 February 2026 doi:10.20944/preprints202602.1018.v1

25. Wang, H.; Guan, H.; Xu, X.; Gao, L.; Gutiérrez-Jurado, H.A.; Simmons, C.T. Topographic Regulations on Ecohydrological Dynamics in a Montane Forest Catchment and the Implications for Plant Adaptation to Environment. *Journal of Hydrology* **2024**, *637*, 131412, doi:10.1016/j.jhydrol.2024.131412.
26. Cartwright, J.M.; Littlefield, C.E.; Michalak, J.L.; Lawler, J.J.; Dobrowski, S.Z. Topographic, Soil, and Climate Drivers of Drought Sensitivity in Forests and Shrublands of the Pacific Northwest, USA. *Sci Rep* **2020**, *10*, 18486, doi:10.1038/s41598-020-75273-5.
27. Xie, X.; Tian, J.; Wu, C.; Li, A.; Jin, H.; Bian, J.; Zhang, Z.; Nan, X.; Jin, Y. Long-Term Topographic Effect on Remotely Sensed Vegetation Index-Based Gross Primary Productivity (GPP) Estimation at the Watershed Scale. *International Journal of Applied Earth Observation and Geoinformation* **2022**, *108*, 102755, doi:10.1016/j.jag.2022.102755.
28. Zhang, Y.; Zhang, C.; Wang, Z.; Chen, Y.; Gang, C.; An, R.; Li, J. Vegetation Dynamics and Its Driving Forces from Climate Change and Human Activities in the Three-River Source Region, China from 1982 to 2012. *Sci Total Environ* **2016**, *563–564*, 210–220, doi:10.1016/j.scitotenv.2016.03.223.
29. Wang, B.; Cheng, W.; Xu, H.; Wang, R.; Song, K.; Bao, A.; Shi, Q. Vegetation Differentiation Characteristics and Control Mechanisms in the Altay Region Based on Topographic Gradients. *Ecological Indicators* **2024**, *160*, 111838, doi:10.1016/j.ecolind.2024.111838.
30. Zou, L.; Tian, F.; Liang, T.; Eklundh, L.; Tong, X.; Tagesson, T.; Dou, Y.; He, T.; Liang, S.; Fensholt, R. Assessing the Upper Elevational Limits of Vegetation Growth in Global High-Mountains. *Remote Sensing of Environment* **2023**, *286*, 113423, doi:10.1016/j.rse.2022.113423.
31. Liang, T.; Tian, F.; Zou, L.; Jin, H.; Tagesson, T.; Rumpf, S.; He, T.; Liang, S.; Fensholt, R. Global Assessment of Vegetation Patterns along Topographic Gradients. *International Journal of Digital Earth* **2024**, *17*, 2404232, doi:10.1080/17538947.2024.2404232.
32. Bai, D.; Wang, Y.; Ma, Y.; Li, H.; Guan, X. Fine-Scale Variations and Driving Factors of GPP Derived from Multi-Source Data Fusion in the Mountainous Region of Northwestern Hubei. *Remote Sensing* **2025**, *17*, 2186, doi:10.3390/rs17132186.
33. Li, Y.; Zhou, S.; Hou, Y.; Hu, Y.; Chen, C.; Liu, Y.; Yuan, L.; Cao, H.; Qian, B.; Liu, Y.; et al. Vegetation Net Primary Productivity Dynamics over the Past Three Decades and Elevation–Climate Synergistic Driving Mechanism in Southwest China's Mountains. *Forests* **2025**, *16*, 919, doi:10.3390/f16060919.
34. Gxasheka, M.; Gajana, C.S.; Dlamini, P. The Role of Topographic and Soil Factors on Woody Plant Encroachment in Mountainous Rangelands: A Mini Literature Review. *Heliyon* **2023**, *9*, e20615, doi:10.1016/j.heliyon.2023.e20615.
35. Li, C.; Jin, Z.; Jiang, C.; Shen, Y.; Wang, R.; Peng, J. How Topographic and Pedological Factors Affect Vegetation Responses to Drought: A Study from the Qinling Mountains, China. *CATENA* **2025**, *260*, 109470, doi:10.1016/j.catena.2025.109470.
36. Xie, S.; Mo, X.; Hu, S.; Liu, S. Contributions of Climate Change, Elevated Atmospheric CO2 and Human Activities to ET and GPP Trends in the Three-North Region of China. *Agricultural and Forest Meteorology* **2020**, *295*, 108183, doi:10.1016/j.agrformet.2020.108183.
37. Yao, B.; Gong, X.; Li, Y.; Li, Y.; Lian, J.; Wang, X. Spatiotemporal Variation and GeoDetector Analysis of NDVI at the Northern Foothills of the Yinshan Mountains in Inner Mongolia over the Past 40 Years. *Heliyon* **2024**, *10*, e39309, doi:10.1016/j.heliyon.2024.e39309.
38. Zhang, M.; Deng, Y.; Hai, Y.; Chen, H.; Ma, A.; Wang, W.; Ming, L.; Dang, H.; Peng, M.; Jize, D.; et al. Monitoring Vegetation Dynamics and Driving Forces in the Baijiu Golden Triangle Using Multi-Decadal Landsat NDVI and Geodetector Modeling. *Land* **2025**, *14*, 1111, doi:10.3390/land14051111.
39. Gu, Z.; Chen, X.; Ruan, W.; Zheng, M.; Gen, K.; Li, X.; Deng, H.; Chen, Y.; Liu, M. Quantifying the Direct and Indirect Effects of Terrain, Climate and Human Activity on the Spatial Pattern of kNDVI-Based Vegetation Growth: A Case Study from the Minjiang River Basin, Southeast China. *Ecological Informatics* **2024**, *80*, 102493, doi:10.1016/j.ecoinf.2024.102493.
40. Guo, X.; Wang, T.; Li, Z.; Cheng, S.; Li, P.; Li, H.; Zhang, N.; Liu, X.; Miao, Z. Using PLE-SEM to Quantify the Impacts of Natural and Human Factors on Vegetation Change: A Case Study of the Jialing River Basin. *Sustainability* **2023**, *15*, 13089, doi:10.3390/su151713089.

© 2025 by the author(s). Distributed under a Creative Commons CC BY license.

Preprints.org (www.preprints.org) | NOT PEER-REVIEWED | Posted: 12 February 2026 doi:10.20944/preprints202602.1018.v1

41. Guo, Y.; Cheng, L.; Ding, A.; Yuan, Y.; Li, Z.; Hou, Y.; Ren, L.; Zhang, S. Geodetector Model-Based Quantitative Analysis of Vegetation Change Characteristics and Driving Forces: A Case Study in the Yongding River Basin in China. *International Journal of Applied Earth Observation and Geoinformation* **2024**, *132*, 104027, doi:10.1016/j.jag.2024.104027.
42. Kang, Y.; Wang, Z.; Xu, B.; Shen, W.; Chen, Y.; Zhou, X.; Liu, Y.; Zhang, T.; Wang, G.; Jia, Y.; et al. Disentangling the Response of Vegetation Dynamics to Natural and Anthropogenic Drivers over the Minjiang River Basin Using Dimensionality Reduction and a Structural Equation Model. *Forests* **2024**, *15*, 1438, doi:10.3390/f15081438.
43. Cui, G.; Wang, Y.; Pugnaire, F.I.; Zhang, L. Non-Linear Responses of Plants Enhance Their Resistance to Drought in Drylands. *TIG* **2025**, *3*, 100136–2, doi:10.59717/j.xinn-geo.2025.100136.
44. Piao, Z.; Li, X.; Xu, H.; Wang, K.; Tang, S.; Kan, F.; Hong, S. Threshold of Climate Extremes That Impact Vegetation Productivity over the Tibetan Plateau. *Sci. China Earth Sci.* **2024**, *67*, 1967–1977, doi:10.1007/s11430-023-1262-y.
45. Beigaitė, R.; Tang, H.; Bryn, A.; Skarpaas, O.; Stordal, F.; Bjerke, J.W.; Žliobaitė, I. Identifying Climate Thresholds for Dominant Natural Vegetation Types at the Global Scale Using Machine Learning: Average Climate versus Extremes. *Global Change Biology* **2022**, *28*, 3557–3579, doi:10.1111/gcb.16110.
46. Ingrisch, J.; Umlauf, N.; Bahn, M. Functional Thresholds Alter the Relationship of Plant Resistance and Recovery to Drought. *Ecology* **2023**, *104*, e3907, doi:10.1002/ecy.3907.
47. Osland, M.J.; Bradford, J.B.; Toth, L.T.; Germino, M.J.; Grace, J.B.; Drexler, J.Z.; Stagg, C.L.; Grossman, E.R.; Thorne, K.M.; Romañach, S.S.; et al. Ecological Thresholds and Transformations Due to Climate Change: The Role of Abiotic Stress. *Ecosphere* **2025**, *16*, e70229, doi:10.1002/ecs2.70229.
48. Li, X.; Xiao, J. Mapping Photosynthesis Solely from Solar-Induced Chlorophyll Fluorescence: A Global, Fine-Resolution Dataset of Gross Primary Production Derived from OCO-2. *Remote Sensing* **2019**, *11*, 2563, doi:10.3390/rs11212563.
49. Ding, H.; Yuan, Z.; Shi, X.; Yin, J.; Chen, F.; Shi, M.; Zhang, F. Soil Moisture Content-Based Analysis of Terrestrial Ecosystems in China: Water Use Efficiency of Vegetation Systems. *Ecological Indicators* **2023**, *150*, 110271, doi:10.1016/j.ecolind.2023.110271.
50. Qi, G.; She, D.; Xia, J.; Song, J.; Jiao, W.; Li, J.; Liu, Z. Soil Moisture Plays an Increasingly Important Role in Constraining Vegetation Productivity in China over the Past Two Decades. *Agricultural and Forest Meteorology* **2024**, *356*, 110193, doi:10.1016/j.agrformet.2024.110193.
51. Mu, B.; Zhao, X.; Wu, D.; Wang, X.; Zhao, J.; Wang, H.; Zhou, Q.; Du, X.; Liu, N. Vegetation Cover Change and Its Attribution in China from 2001 to 2018. *Remote Sensing* **2021**, *13*, 496, doi:10.3390/rs13030496.
52. Zhu, Z.; Piao, S.; Myneni, R.B.; Huang, M.; Zeng, Z.; Canadell, J.G.; Ciais, P.; Sitch, S.; Friedlingstein, P.; Arneth, A.; et al. Greening of the Earth and Its Drivers. *Nature Clim Change* **2016**, *6*, 791–795, doi:10.1038/nclimate3004.
53. Zhou, W.; Li, C.; Fu, B.; Wang, S.; Ren, Z.; Stringer, L.C. Changes and Drivers of Vegetation Productivity in China's Drylands under Climate Change. *Environ. Res. Lett.* **2024**, *19*, 114001, doi:10.1088/1748-9326/ad7a0e.
54. Liu, S.; Yang, D.; Zhang, X.; Liu, F. Quantitative Analysis and Nonlinear Response of Vegetation Dynamic to Driving Factors in Arid and Semi-Arid Regions of China. *Land* **2025**, *14*, 1575, doi:10.3390/land14081575.
55. Peng, J.; Xue, Y.; Pan, N.; Zhang, Y.; Liang, H.; Zhang, F. Exploring the Spatiotemporal Alterations in China's GPP Based on the DTEC Model. *Remote Sensing* **2024**, *16*, 1361, doi:10.3390/rs16081361.
56. Kooistra, L.; Berger, K.; Brede, B.; Graf, L.V.; Aasen, H.; Roujean, J.-L.; Machwitz, M.; Schlerf, M.; Atzberger, C.; Prikaziuk, E.; et al. Reviews and Syntheses: Remotely Sensed Optical Time Series for Monitoring Vegetation Productivity. *Biogeosciences* **2024**, *21*, 473–511, doi:10.5194/bg-21-473-2024.
57. Li, Y.; Zhou, S.; Hou, Y.; Hu, Y.; Chen, C.; Liu, Y.; Yuan, L.; Cao, H.; Qian, B.; Liu, Y.; et al. Vegetation Net Primary Productivity Dynamics over the Past Three Decades and Elevation–Climate Synergistic Driving Mechanism in Southwest China's Mountains. *Forests* **2025**, *16*, 919, doi:10.3390/f16060919.
58. Chen, Y.; Gu, H.; Wang, M.; Gu, Q.; Ding, Z.; Ma, M.; Liu, R.; Tang, X. Contrasting Performance of the Remotely-Derived GPP Products over Different Climate Zones across China. *Remote Sensing* **2019**, *11*, 1855, doi:10.3390/rs11161855.

© 2025 by the author(s). Distributed under a Creative Commons CC BY license.

Preprints.org (www.preprints.org) | NOT PEER-REVIEWED | Posted: 12 February 2026 doi:10.20944/preprints202602.1018.v1

59. Li, C.; Zhang, Y.; Liu, Y.; Wu, J.; Wang, A. Temporal and Spatial Variations and Influencing Factors of Gross Primary Productivity in Changbai Mountain Nature Reserve, China. *Chinese Journal of Applied Ecology* **2023**, *34*, 1341, doi:10.13287/j.1001-9332.202305.026.
60. Schuur, E.A.; Matson, P.A. Net Primary Productivity and Nutrient Cycling across a Mesic to Wet Precipitation Gradient in Hawaiian Montane Forest. *Oecologia* **2001**, *128*, 431–442, doi:10.1007/s004420100671.
61. Zhong, R.; Wang, P.; Mao, G.; Chen, A.; Liu, J. Spatiotemporal Variation of Enhanced Vegetation Index in the Amazon Basin and Its Response to Climate Change. *Physics and Chemistry of the Earth, Parts A/B/C* **2021**, *123*, 103024, doi:10.1016/j.pce.2021.103024.
62. Xu, M.; Zhang, Z.; Wang, Y.; Liu, B. Quantifying the Contributions of Climatic and Human Factors to Vegetation Net Primary Productivity Dynamics in East Africa. *Front. For. Glob. Change* **2024**, *6*, doi:10.3389/ffgc.2023.1332631.
63. Wei, D.; Qi, Y.; Ma, Y.; Wang, X.; Ma, W.; Gao, T.; Huang, L.; Zhao, H.; Zhang, J.; Wang, X. Plant Uptake of CO2 Outpaces Losses from Permafrost and Plant Respiration on the Tibetan Plateau. *Proceedings of the National Academy of Sciences* **2021**, *118*, e2015283118, doi:10.1073/pnas.2015283118.
64. Alfaro-Sánchez, R.; Richardson, A.D.; Smith, S.L.; Johnstone, J.F.; Turetsky, M.R.; Cumming, S.G.; Le Moine, J.M.; Baltzer, J.L. Permafrost Instability Negates the Positive Impact of Warming Temperatures on Boreal Radial Growth. *Proceedings of the National Academy of Sciences* **2024**, *121*, e2411721121, doi:10.1073/pnas.2411721121.
65. Mehmood, K.; Anees, A.; Rehman, A.; Rehman, N.; Shahzad, F.; Liu, Q.; Alharbi, A.; Alfarraj, S.; Ansari, M.; Khan, W. Assessment of Climatic Influences on Net Primary Productivity along Elevation Gradients in Temperate Ecoregions. *Trees Forests and People* **2024**, *18*, doi:10.1016/j.tfp.2024.100657.
66. Sun, C.; Hou, H.; Chen, W. Effects of Vegetation Cover and Slope on Soil Erosion in the Eastern Chinese Loess Plateau under Different Rainfall Regimes. *PeerJ* **2021**, *9*, e11226, doi:10.7717/peerj.11226.
67. Pan, J.; Sharif, R.; Xu, X.; Chen, X. Mechanisms of Waterlogging Tolerance in Plants: Research Progress and Prospects. *Front. Plant Sci.* **2021**, *11*, doi:10.3389/fpls.2020.627331.
68. McNichol, B.H.; Wang, R.; Hefner, A.; Helzer, C.; McMahon, S.M.; Russo, S.E. Topography-Driven Microclimate Gradients Shape Forest Structure, Diversity, and Composition in a Temperate Refugial Forest. *Plant-Environment Interactions* **2024**, *5*, e10153, doi:10.1002/pei3.10153.
69. Ma, Z.; Dong, C.; Tang, Z.; Wang, N. Altitude-Dependent Responses of Dryland Mountain Ecosystems to Drought under a Warming Climate in the Qilian Mountains, NW China. *Journal of Hydrology* **2024**, *630*, 130763, doi:10.1016/j.jhydrol.2024.130763.
70. Wei, D.; Tao, J.; Wang, Z.; Zhao, H.; Zhao, W.; Wang, X. Elevation-Dependent Pattern of Net CO2 Uptake across China. *Nat Commun* **2024**, *15*, 2489, doi:10.1038/s41467-024-46930-4.
71. Zhao, Y.; Wang, L.; Jiang, Q.; Wang, Z. Sensitivity of Gross Primary Production to Precipitation and the Driving Factors in China's Agricultural Ecosystems. *Science of The Total Environment* **2024**, *948*, 174938, doi:10.1016/j.scitotenv.2024.174938.
72. Nemani, R.R.; Keeling, C.D.; Hashimoto, H.; Jolly, W.M.; Piper, S.C.; Tucker, C.J.; Myneni, R.B.; Running, S.W. Climate-Driven Increases in Global Terrestrial Net Primary Production from 1982 to 1999. *Science* **2003**, *300*, 1560–1563, doi:10.1126/science.1082750.
73. Seddon, A.W.R.; Macias-Fauria, M.; Long, P.R.; Benz, D.; Willis, K.J. Sensitivity of Global Terrestrial Ecosystems to Climate Variability. *Nature* **2016**, *531*, 229–232, doi:10.1038/nature16986.
74. Körner, C. A Re-Assessment of High Elevation Treeline Positions and Their Explanation. *Oecologia* **1998**, *115*, 445–459, doi:10.1007/s004420050540.
75. Tromp-van Meerveld, H.J.; McDonnell, J.J. Threshold Relations in Subsurface Stormflow: 2. The Fill and Spill Hypothesis. *Water Resources Research* **2006**, *42*, doi:10.1029/2004WR003800.
76. Amatulli, G.; Domisch, S.; Tuanmu, M.-N.; Parmentier, B.; Ranipeta, A.; Malczyk, J.; Jetz, W. A Suite of Global, Cross-Scale Topographic Variables for Environmental and Biodiversity Modeling. *Sci Data* **2018**, *5*, 180040, doi:10.1038/sdata.2018.40.
77. Wang, P.; Huang, K.; Hu, S. Distinct Fine-Root Responses to Precipitation Changes in Herbaceous and Woody Plants: A Meta-Analysis. *New Phytologist* **2020**, *225*, 1491–1499, doi:10.1111/nph.16266.

© 2025 by the author(s). Distributed under a Creative Commons CC BY license.

Preprints.org (www.preprints.org) | NOT PEER-REVIEWED | Posted: 12 February 2026 doi:10.20944/preprints202602.1018.v1

78. Wang, J.; Taylor, A.R.; D'Orangeville, L. Warming-Induced Tree Growth May Help Offset Increasing Disturbance across the Canadian Boreal Forest. *Proceedings of the National Academy of Sciences* **2023**, *120*, e2212780120, doi:10.1073/pnas.2212780120.
79. Peñuelas, J.; Ciais, P.; Canadell, J.G.; Janssens, I.A.; Fernández-Martínez, M.; Carnicer, J.; Obersteiner, M.; Piao, S.; Vautard, R.; Sardans, J. Shifting from a Fertilization-Dominated to a Warming-Dominated Period. *Nat Ecol Evol* **2017**, *1*, 1438–1445, doi:10.1038/s41559-017-0274-8.
80. Huang, M.; Piao, S.; Ciais, P.; Peñuelas, J.; Wang, X.; Keenan, T.F.; Peng, S.; Berry, J.A.; Wang, K.; Mao, J.; et al. Air Temperature Optima of Vegetation Productivity across Global Biomes. *Nat Ecol Evol* **2019**, *3*, 772–779, doi:10.1038/s41559-019-0838-x.
81. Yuan, W.; Zheng, Y.; Piao, S.; Ciais, P.; Lombardozzi, D.; Wang, Y.; Ryu, Y.; Chen, G.; Dong, W.; Hu, Z.; et al. Increased Atmospheric Vapor Pressure Deficit Reduces Global Vegetation Growth. *Science Advances* **2019**, *5*, eaax1396, doi:10.1126/sciadv.aax1396.
82. Grossiord, C.; Buckley, T.N.; Cernusak, L.A.; Novick, K.A.; Poulter, B.; Siegwolf, R.T.W.; Sperry, J.S.; McDowell, N.G. Plant Responses to Rising Vapor Pressure Deficit. *New Phytologist* **2020**, *226*, 1550–1566, doi:10.1111/nph.16485.
83. Humphrey, V.; Berg, A.; Ciais, P.; Gentine, P.; Jung, M.; Reichstein, M.; Seneviratne, S.I.; Frankenberg, C. Soil Moisture–Atmosphere Feedback Dominates Land Carbon Uptake Variability. *Nature* **2021**, *592*, 65–69, doi:10.1038/s41586-021-03325-5.
84. Jiao, W.; Wang, L.; Smith, W.K.; Chang, Q.; Wang, H.; D'Odorico, P. Observed Increasing Water Constraint on Vegetation Growth over the Last Three Decades. *Nat Commun* **2021**, *12*, 3777, doi:10.1038/s41467-021-24016-9.
85. Knohl, A.; Baldocchi, D.D. Effects of Diffuse Radiation on Canopy Gas Exchange Processes in a Forest Ecosystem. *Journal of Geophysical Research: Biogeosciences* **2008**, *113*, doi:10.1029/2007JG000663.
86. Liu, L.; Gudmundsson, L.; Hauser, M.; Qin, D.; Li, S.; Seneviratne, S.I. Soil Moisture Dominates Dryness Stress on Ecosystem Production Globally. *Nat Commun* **2020**, *11*, 4892, doi:10.1038/s41467-020-18631-1.
87. Reichstein, M.; Bahn, M.; Ciais, P.; Frank, D.; Mahecha, M.D.; Seneviratne, S.I.; Zscheischler, J.; Beer, C.; Buchmann, N.; Frank, D.C.; et al. Climate Extremes and the Carbon Cycle. *Nature* **2013**, *500*, 287–295, doi:10.1038/nature12350.

Disclaimer/Publisher's Note: The statements, opinions and data contained in all publications are solely those of the individual author(s) and contributor(s) and not of MDPI and/or the editor(s). MDPI and/or the editor(s) disclaim responsibility for any injury to people or property resulting from any ideas, methods, instructions or products referred to in the content.

© 2025 by the author(s). Distributed under a Creative Commons CC BY license.